On the role of the pre-exposure time in the stress-corrosion cracking of magnesium alloys

Evgeniy Merson[1*], Vitaliy Poluyanov[1], Pavel Myagkikh[1], Dmitri Merson[1], Alexei Vinogradov [2]

[1]*Institute of Advanced Technologies, Togliatti State University, Belorusskaya str. 14, Togliatti 445667, Russian Federation*

[2]*Department of Mechanical and Industrial Engineering, Norwegian University of Science and Technology – NTNU, N-7491 Trondheim, Norway*

**Email: mersoned@gmail.com*

Pre-exposure of Mg alloys to corrosive media causes their embrittlement, which has been long associated with diffusible hydrogen penetrating into the metal. The time of the pre-exposure was suggested to promote embrittlement due to increasing both the corrosion damage and hydrogen concentration. However, recently it was shown that removal of corrosion products from the pre-exposed specimens results in full elimination of the all harmful effects induced by pre-exposure. This observation casts doubts about the significance of diffusible hydrogen in pre-exposure embrittlement. In view of those new findings, the effect of pre-exposure time on the embrittlement phenomenon is revisited in the present study. The specimens of the ZK60 and AZ31 alloys were pre-exposed to 4% NaCl + 4% $K_2Cr_2O_7$ corrosive media for different durations and then slow-strain rate tensile tested in air either as are or after removal of corrosion products. It is found that the pre-exposure embrittlement of both alloys increases with the increasing pre-exposure time and is caused by the cooperative effect of the corrosion damage and the brittle cracking mechanism. The latter is (i) activated by the deposition of the essentially thick corrosion products layer on the specimen surface during pre-exposure, (ii) promoted by the increasing amount of corrosion products and (iii) can be fully inhibited by the removal of corrosion products from the specimen surface. The corrosion damage produces the irreversible loss in ductility and strength, which becomes more pronounced with the increasing pre-exposure time, but it does not alternate the fracture mode. No evidence is found for the increasing concentration of diffusible hydrogen in Mg alloys with the increasing pre-exposure time.

Keywords: Mg alloys; stress corrosion cracking; pre-exposure embrittlement; gas-analysis; slow-strain rate tensile testing; quantitative fractography

1. Introduction

Stress corrosion cracking (SCC) is a root cause for sudden brittle failures of metallic components under the combined action of mechanical in-service loads and the aggressive environment. In particular, SCC is a crucial issue impeding the broader spread of magnesium alloys [1–3], which have been in increasing demand by industry and medicine in recent years [4–6]. The improvement of corrosion and SCC resistance of Mg alloys is still a challenging task, largely because of insufficient understanding of the complicated mechano-chemical interactions responsible for the environmentally-assisted fracture of these materials. An extensive study of this topic promoted a widely accepted viewpoint that along with the conventional anodic dissolution, hydrogen plays a pivotal role in SCC of Mg [1,7]. Hydrogen was suggested to cause the embrittlement of Mg alloys through several possible ways, including (i) the formation of brittle hydrides (*delayed hydride cracking* – DHC) [8–12], (ii) reduction of inter-atomic bonds followed by the decohesion along crystallographic planes (*hydrogen-enhanced decohesion* – HEDE) [11–13], (iii) the enhancement of dislocation movement in the local volumes (*hydrogen-enhanced localised plasticity* – HELP) [11,12] and (iv) the promoting crack growth by the adsorption-induced facilitation of dislocation emission from the crack tip (*adsorption-induced dislocation emission* – AIDE) [14]. Except for the latter one, all these mechanisms appeal to diffusible hydrogen, i.e. the hydrogen possessing substantial mobility at room temperature to be rapidly redistributed within the bulk metal and to be accumulated at high concentration in the local volumes. It is believed that diffusible hydrogen is supplied into Mg matrix via the cathodic reaction, which is an intrinsic part of the corrosion process. Among the existing arguments in favour of this belief, a fact to be mentioned is that the specimens pre-exposed to corrosive media suffer from SCC during the subsequent slow-strain rate tensile (SSRT) testing in air. For the first time, such the effect referred to as *pre-exposure embrittlement* or SCC was documented by Chakrapani and Pugh who conducted the tensile testing of the high-purity binary Mg-7.5Al alloy pre-exposed to the 4% NaCl – 4% $KCrO_4$ solution [9]. Afterwards, the pre-exposure SCC has been reported for commercial and high purity magnesium [15] as well as for various Mg-based alloys including AZ31 [16,17], AZ80 [18], Mg-9Al [19], ZK21 [20] and Mg-Zn-Y-Zr [21]. In all these cited papers, the observed embrittlement phenomenon was unanimously attributed to the hydrogen absorbed by the metal during the pre-exposure process. In support of this conclusion, many authors have shown that the embrittlement became more severe with the increasing pre-exposure time ranging from 2.5 up to 96 h [9,16–20]. It was suggested in refs. [9,16–20] and experimentally evidenced by the melt-extraction gas-analysis in ref. [9] that the longer pre-exposure time results in the enhanced concentration of hydrogen in the base metal [9,16–20].

Besides, vacuum annealing [9] or desiccator storing [17] of pre-exposed specimens leads to partial recovery of their mechanical properties. This was considered as further supporting evidence for the claim that hydrogen embrittlement caused by diffusible hydrogen as the latter is known to escape from the metal at room and elevated temperatures. On the other hand, the remaining after the ageing loss in strength and ductility was attributed either to corrosion damage produced by anodic dissolution [9,17] or to molecular hydrogen strongly trapped in voids [9].

Noteworthy is that Merson et al. [22] have recently demonstrated that the removal of corrosion products from the specimens of the ZK60 alloy severely embrittled by 1.5 hours pre-exposure to corrosive solutions of different compositions results in complete recovery of the metal's ductility. This finding casts doubts on the significance of diffusible hydrogen in the mechanism of the pre-exposure SCC and motivated the present research. Indeed, the removal of corrosion products can hardly cause the complete desorption of hydrogen from the base metal (if hydrogen had been absorbed by the metal at all). Nevertheless, it can be supposed that 1.5 h pre-exposure was not long enough for hydrogen to diffuse deeply into the bulk. Thus, there could be not enough time to buildup the essential hydrogen concentration in the volume. As opposes to this, the hydrogen sitting in the subsurface layer can possibly escape into the atmosphere after removal of corrosion products, which presumably serve as the barrier for diffusible hydrogen. Although the 1.5 h pre-exposure time was enough to induce the severe ductility loss in the alloy, the considerably longer pre-exposure duration ranging typically from 2.5 up to 95 h has been adopted in other studies. Thus, aiming at verifying the findings reported in [22] and getting new insights into the mechanism of SCC in Mg-based alloys, the objective of the present study is to investigate the effect of the pre-exposure time on the mechanical properties, hydrogen concentration, corrosion damage and fractographic features of Mg alloys submerged in corrosive media, and, then, SSRT tested in air after removal of corrosion products.

2. Experimental

The hot-extruded commercial alloy ZK60 and the hot-rolled commercial AZ31 were used. Their chemical compositions represented in Table 1 were the same as those used in our companion studies [22–24]. The microstructure of the ZK60 and AZ31 alloys is composed of equiaxed grains of 3 and 10 μm, respectively. Metallographic data and the detailed description of these microstructures are provided elsewhere [23]. The threaded round specimens with the gauge part of 6 mm diameter and 30 mm length were machined along the extrusion or rolling directions for ZK60 and AZ31, respectively. The gauge parts of the specimens were grinded by emery paper down to grade 2500. For the gas-analysis and the corrosion damage assessment, the samples of 30 mm length and 6 mm diameter were machined from the shoulder parts of the

specimens fractured during SSRT testing. The size and geometry of these samples mimics the gauge part of the full-scale specimens used for SSRT testing.

Table 1 – Chemical compositions of the investigated alloys (in wt. %)

Material	**Mg**	**Al**	**Zn**	**Ca**	**Zr**	**Fe**	**Cu**	**Mn**	**Ce**	**Nd**	**Si**
ZK60	Balance	0.002	5.417	0.0004	0.471	0.001	0.002	0.005	0.002	0.003	0.003
AZ31		4.473	0.887	0.0015	-	0.002	0.003	0.312	0.017	0.007	0.008

The slow-strain rate tensile (SSRT) testing was conducted at $5.6 \cdot 10^{-6}$ s^{-1} (0.01 mm/min) nominal strain rate using the AG-X Plus (Shimadzu) screw-driven frame. At least two specimens were tested at each specific experimental condition. For reference, several specimens were tested for both alloys in the as-received state in air. The other specimens were pre-exposed to corrosive media. The pre-exposure time was varied from 1.5 to 12 h for the alloy ZK60 and from 6 to 24 h for AZ31. The longer pre-exposure times for the alloy AZ31 were chosen due to its lower susceptibility to SCC. The specimens were submerged into the aqueous solution of 4% NaCl + 4% $K_2Cr_2O_7$ at the open-circuit potential without external mechanical load. It was shown recently that this solution caused the severe and persistent pre-exposure embrittlement of the ZK60 alloy [22]. The SSRT testing was started within 5 minutes after the end of the pre-exposure time. The specimens were cleaned with running water, rinsed with ethanol and dried by paper towels and compressed air. Before SSRT testing, the corrosion products were removed from a part of the pre-exposed specimens by the immersion into the standard 20% CrO_3 + 1%$AgNO_3$ aqueous solution for 1 min followed by rinsing the specimens with ethanol and drying by compressed air. As has been shown in [22], this procedure inhibits SCC effects in the ZK60 specimens pre-exposed for 1.5 h to the various corrosive solutions, including the one used in the present study.

The degree of corrosion damage was assessed by the weight loss method using the small cylindrical samples immersed in the corrosive solution for various times and then subjected to removal of corrosion products. The chemical composition of the corrosive solution, immersion duration and other conditions of the pre-exposure and removal of corrosion products procedures were identical to those used for the full-scale specimens for the SSRT testing. The weights, m, and diameters, d, of the samples before (m_1, d_1) and after (m_2 d_2) immersion as well as after removal of corrosion products (m_3, d_3) were measured with ±0.1 mg and ±0.01 mm accuracy, respectively. Using this data, the weight loss, m_c, the diameter loss, d_c, and the relative weight of corrosion products m_{cp} have been estimated using the equations (1-3), respectively.

$$m_c = \frac{m_1 - m_3}{m_1} \cdot 100\% \quad (1)$$

$$d_c = \frac{d_1 - d_3}{d_1} \cdot 100\% \quad (2)$$

$$m_{cp} = \frac{m_2 - m_3}{m_2} \cdot 100\% \quad (3)$$

After weighting, the corroded samples were subjected to the gas-analysis by the hot-extraction method using the G8 Galileo (Bruker) gas-analyzer as described in refs. [22–24].

The microscopic examination of side and fracture surfaces was performed using the scanning electron microscope (SEM) JCM-6000 (JEOL) and the confocal laser scanning microscope (CLSM) Lext OLS4000 (Olympus). The latter was used also for the areal roughness measurements. The total area and areal fraction of the brittle zone on the fracture surfaces were assessed on the SEM images by manual selection of the region of interest with the use of the ImageJ open source image processing software.

3. Results

3.1.Mechanical testing

The results of SSRT testing showed that the pre-exposure to corrosive media leads to the significant deterioration of mechanical properties of the alloy ZK60, c.f. Fig. 1 and 2. The elongation to failure (EF) of this alloy dropped after 1.5 h pre-exposure, and, then, it gradually decreased further with increasing pre-exposure time up to 12 h, c.f. Fig. 1a. Thus, one has to note that the loss of ductility observed after the first 1.5 h pre-exposure is much more severe than that in the subsequent 10 h. As can be seen from Fig. 2a, the decrease of elongation occurs mainly due to the reduction of the necking part of the stress-strain diagram, although the uniform strain is also compromised. Both the ultimate tensile strength (UTS) and the yield stress (YS) are also significantly reduced with increasing pre-exposure time, c.f. Fig. 1b and 2a. However, the observed reduction of strength occurs more uniformly in comparison with the ductility: the decrease in UTS after 1.5 h pre-exposure is much less pronounced than that in EF.

Compared to ZK60, the alloy AZ31 is notably less susceptible to SCC induced by pre-exposure to 4% NaCl+4% $K_2Cr_2O_7$, c. f. Fig. 1 and Fig. 2c. Although EF of this alloy slightly decreases with increasing pre-exposure time, the ductility loss is much lesser than for ZK60 at all pre-exposure times. UTS and YS values of the AZ31 alloy are virtually not affected by the pre-exposure regardless of its duration. The slight decrease in UTS, which is seen after 6 h pre-exposure, can be likely attributed to the regular experimental scatter.

As it follows from Fig. 1 and 2b, d, the removal of corrosion products from the specimens results in recovery of mechanical properties of both alloys. The ductility of AZ31 specimens can be fully restored by the removal of corrosion products in the whole range of pre-exposure time from 6 to 24 hours, while the strength was not compromised at all. For the alloy ZK60, the rate of the recovery strongly depends on pre-exposure time. In congruence with the results of our recent study [22], the ductility of the ZK60 specimens pre-exposed to corrosive media for 1.5 h fully recovers or even increases slightly after removal of corrosion products. However, if the specimens were pre-exposed to the corrosive media for longer times, the removal of corrosion products did not result in the complete recovery of ductility anymore. Moreover, the healing effect produced by removing corrosion products is reduced strongly when pre-exposure time extends, Fig. 1a. The increase in UTS and YS associated with the removal of corrosion products is much less significant in comparison to that in EF and is almost independent of pre-exposure time.

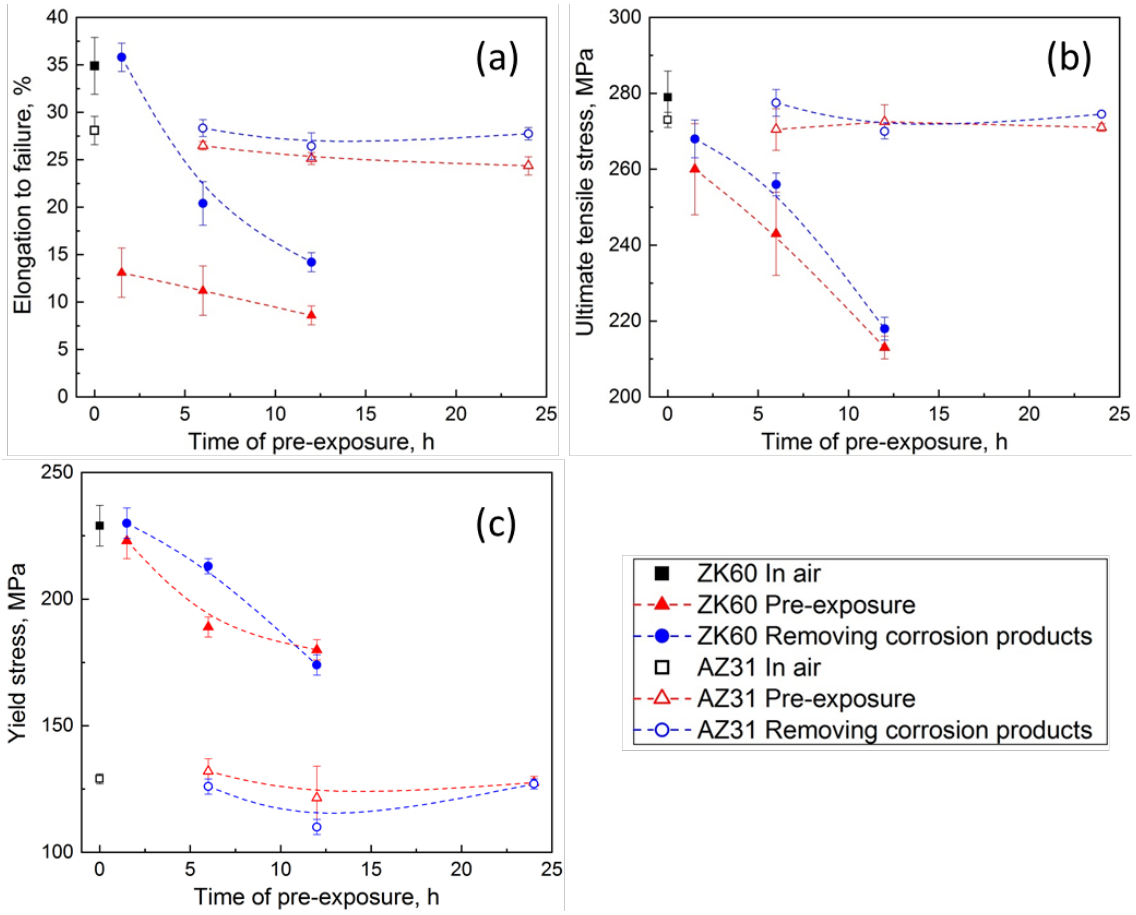

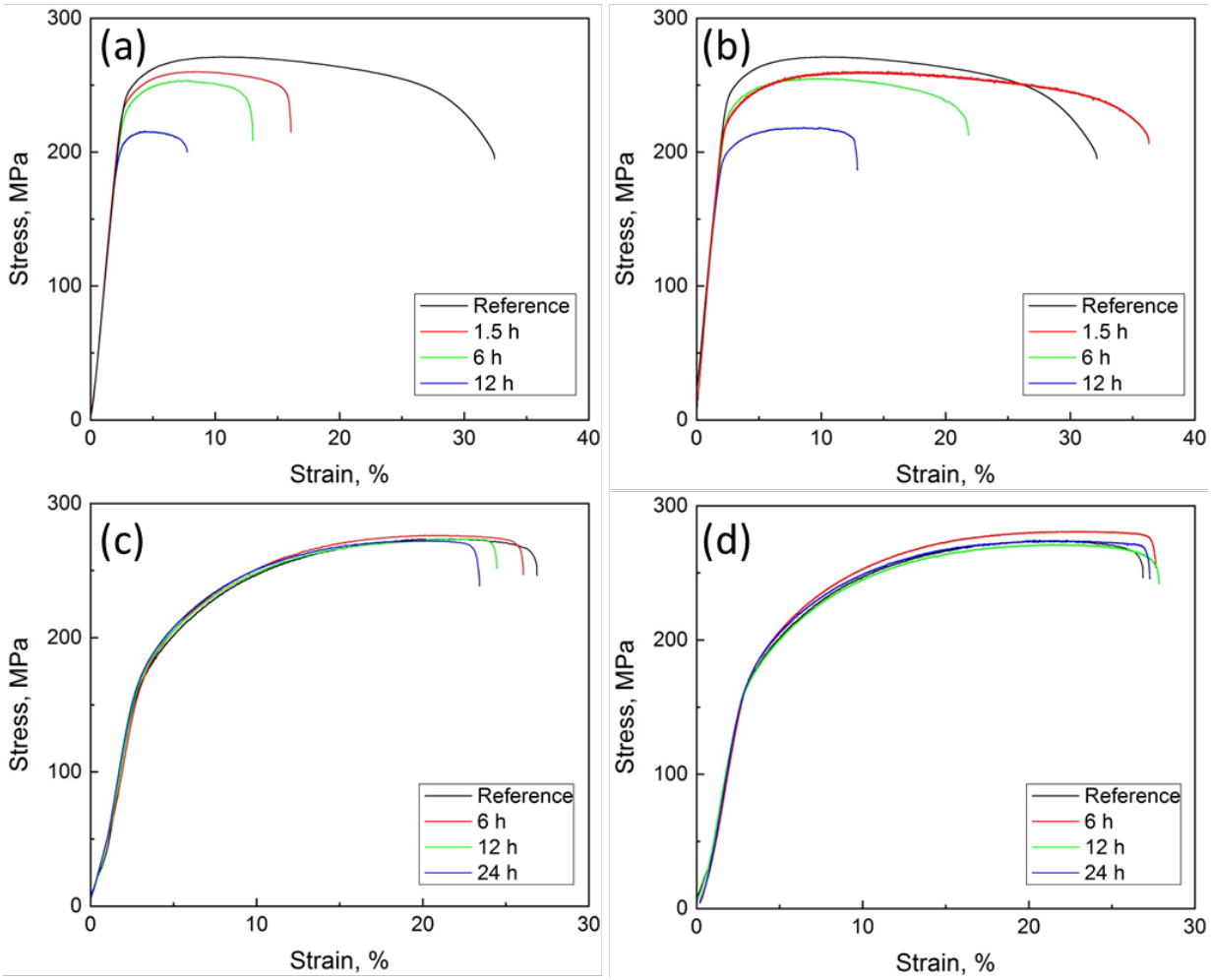

3.2. Side surface analysis

The visual examination of the pre-exposed specimens of both alloys showed that their side surfaces contacted with the corrosive solution were covered by solid films of dark corrosion products, c. f. Figs. 3a, c, e and 4a, c, e. After removal of corrosion products, the surface of the ZK60 specimens appears mainly matt and grey, Fig. 3b, d and f. The side surface of the AZ31 specimens with removed corrosion products is featured by the brown colour, which is the darker, the longer pre-exposure time is, Fig. 4b, d and f. This observation indicates that the corrosion products deposited on the AZ31 specimens are removed less effectively than from ZK60 (the same solution for the removal of corrosion products was used for both alloys). Furthermore, the

amount of corrosion products retaining on the surface of the AZ31 specimens after removal of corrosion products increases with pre-exposure time.

It can be seen by the naked eyes in Fig. 3, as well as on the SEM images in Fig. 5, that the surface of the ZK60 specimens becomes considerably rougher due to corrosion damage as pre-exposure time increases. In contrast, the side surfaces of the AZ31 specimens remain visually undamaged by corrosion even after of 24 hours pre-exposure, c.f. Fig. 4.

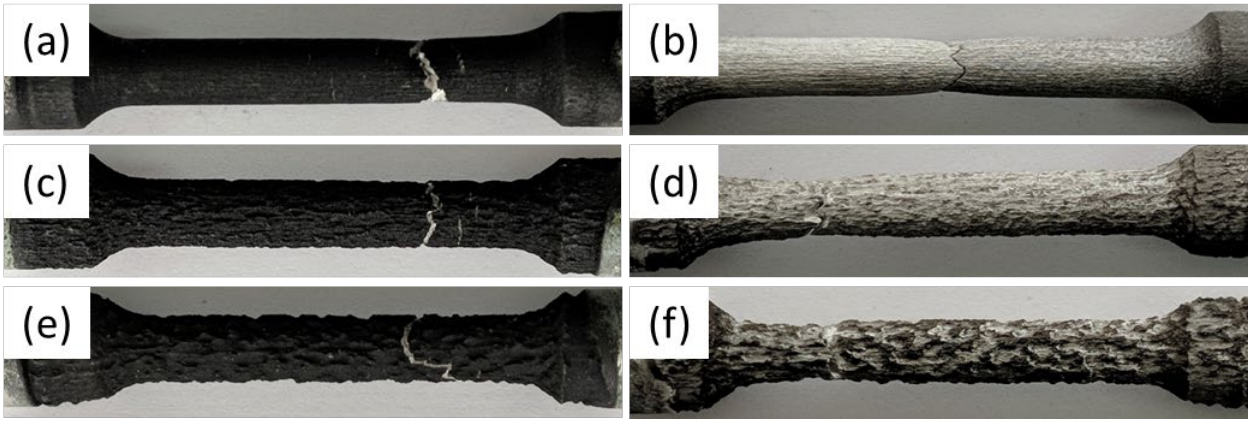

Fig. 3 – The appearance of the ZK60 alloy specimens SSRT tested in air after pre-exposure to 4% NaCl + 4% $K_2Cr_2O_7$ for 1.5 – (a, b), 6 – (c, d) and 12 h – (e, f) either as are – (a, c, e) or after removal of corrosion products – (b, d, f).

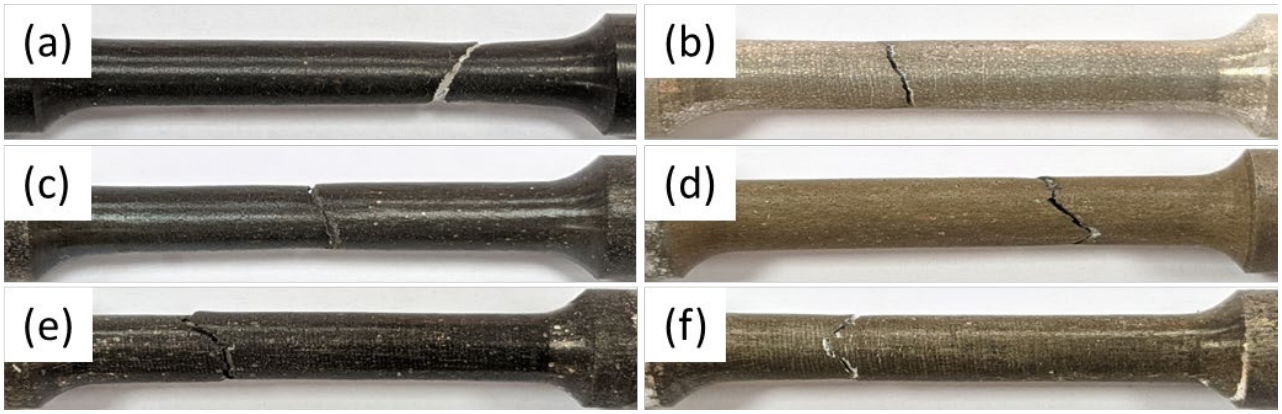

Fig. 4 – The appearance of the AZ31 alloy specimens SSRT tested in air after pre-exposure to 4% NaCl + 4% $K_2Cr_2O_7$ for 6 – (a, b), 12 – (c, d) and 24 h – (e, f) either as are – (a, c, e) or after removal of corrosion products – (b, d, f).

With the aid of SEM, it is found that, for both alloys, the specimens, which were SSRT tested right after pre-exposure, demonstrate numerous side surface cracks on the gauge part, c.f. Fig. 5a-c, Fig. 6a, b, Fig. 7a-c and Fig. 8a, b. The cracks are oriented perpendicularly to the tensile axis and tend to coalesce in a stepwise manner to produce large macroscopic cracks. The

cracks in the alloy ZK60 are considerably deeper, Fig. 5a-c and 6a, b, than in AZ31, Fig. 7a-c and 8a, b, although the number of cracks seems to be comparable for both alloys. Interestingly is that the number of the side surface cracks for the ZK60 specimens decreases with increasing pre-exposure time as is clearly seen in Fig. 5a-c. Such a tendency is not observed for AZ31, c.f. Fig. 7a-c. If the corrosion products were removed from the ZK60 specimens before SSRT testing, the transverse cracks were not formed on the side surface regardless of pre-exposure time, c.f. Fig. 5d-f. Nevertheless, a few ductile shear cracks inclined at 45 degrees to the tensile axis can be found close to the fracture surface, Fig. 6c. At a higher magnification, one can also observe corrosion pits, such as those represented in Fig. 6d. Removing corrosion products does not fully prevent cracking in the AZ31 specimens. However, the number, length and depth of the cracks decrease notably, Fig. 7d-f and 8c, d. Besides, one can notice the prevalence of shear cracking in the specimens with removed corrosion products, whereas transverse cracking is the primary fracture mode in the specimens SSRT tested immediately after pre-exposure.

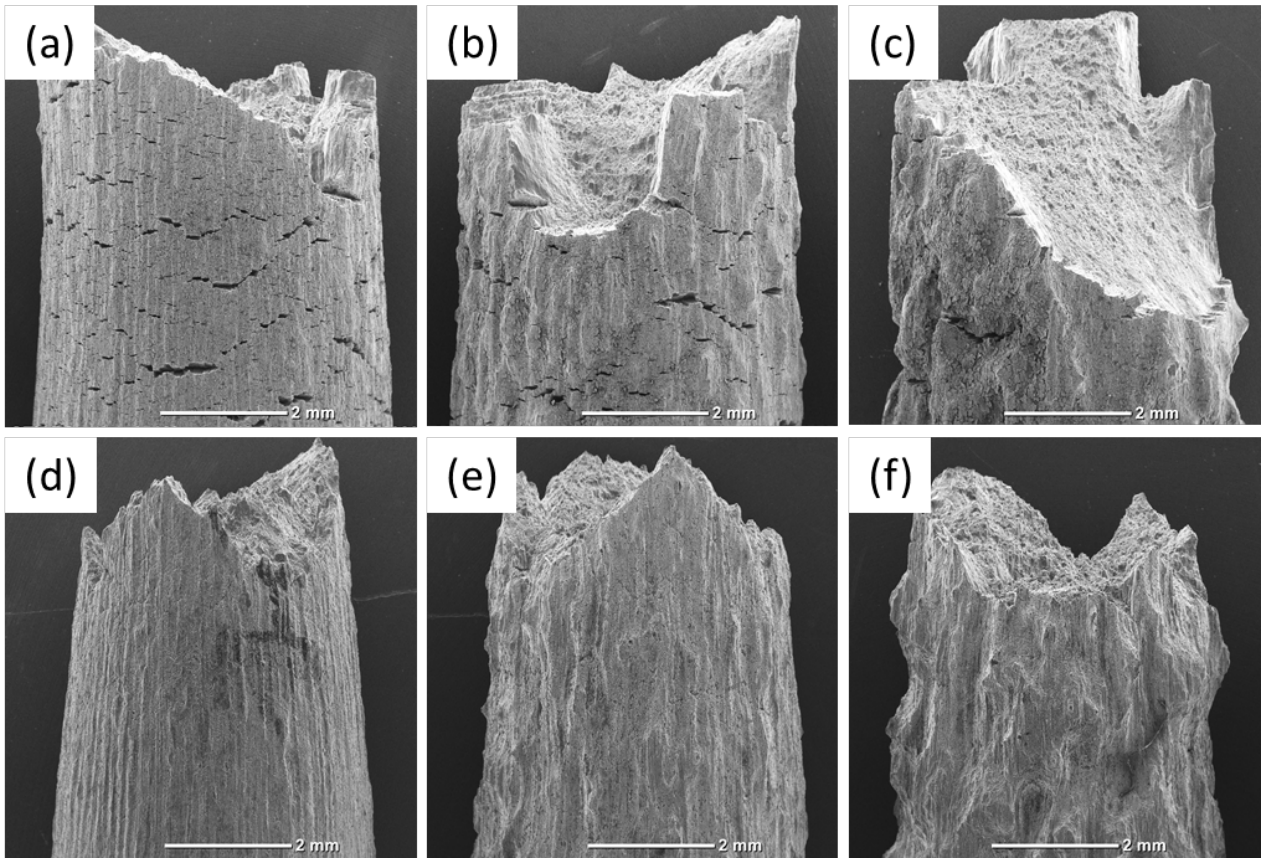

Fig. 5 – The SEM images representing the side surface of the ZK60 alloy specimens SSRT tested in air after pre-exposure to 4% NaCl + 4% $K_2Cr_2O_7$ for 1.5 – (a, d), 6 – (b, e) and 12 h – (c, f) either as are – (a-c) or after removal of corrosion products – (d-f).

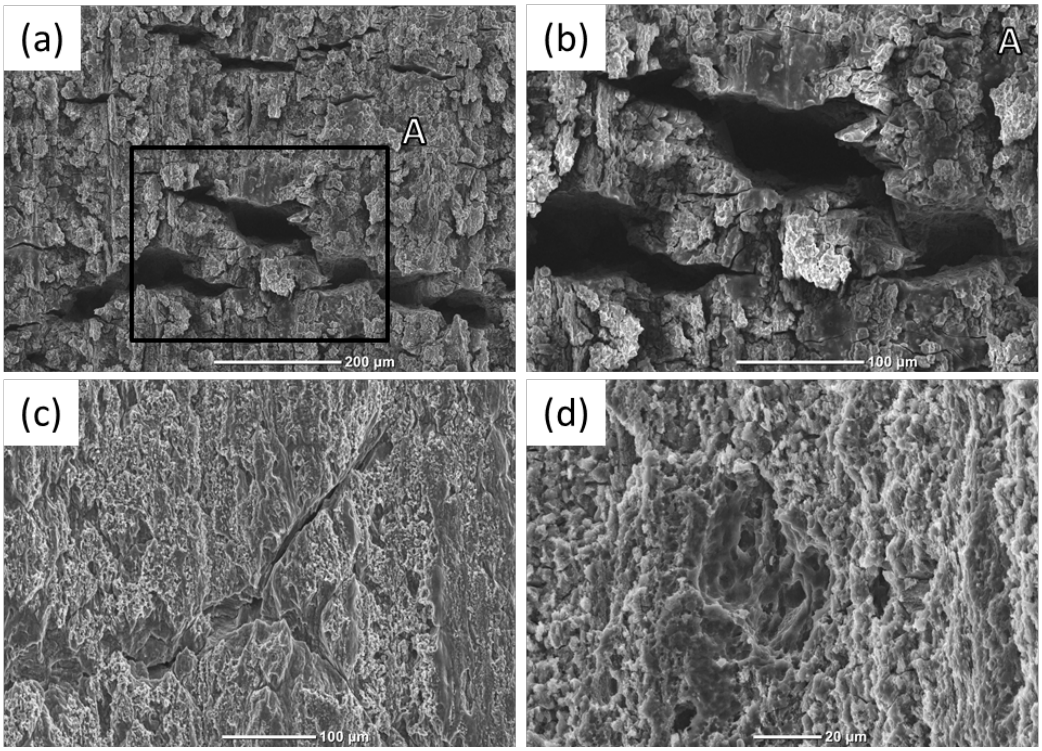

Fig. 6 – The SEM images demonstrating the brittle transverse – (a, b) and ductile shear – (c) cracks and corrosion pits – (d) on the side surface of the ZK60 alloy specimens SSRT tested in air after 1.5 h pre-exposure either as are – (a, b) or after removal of corrosion products – (c, d).

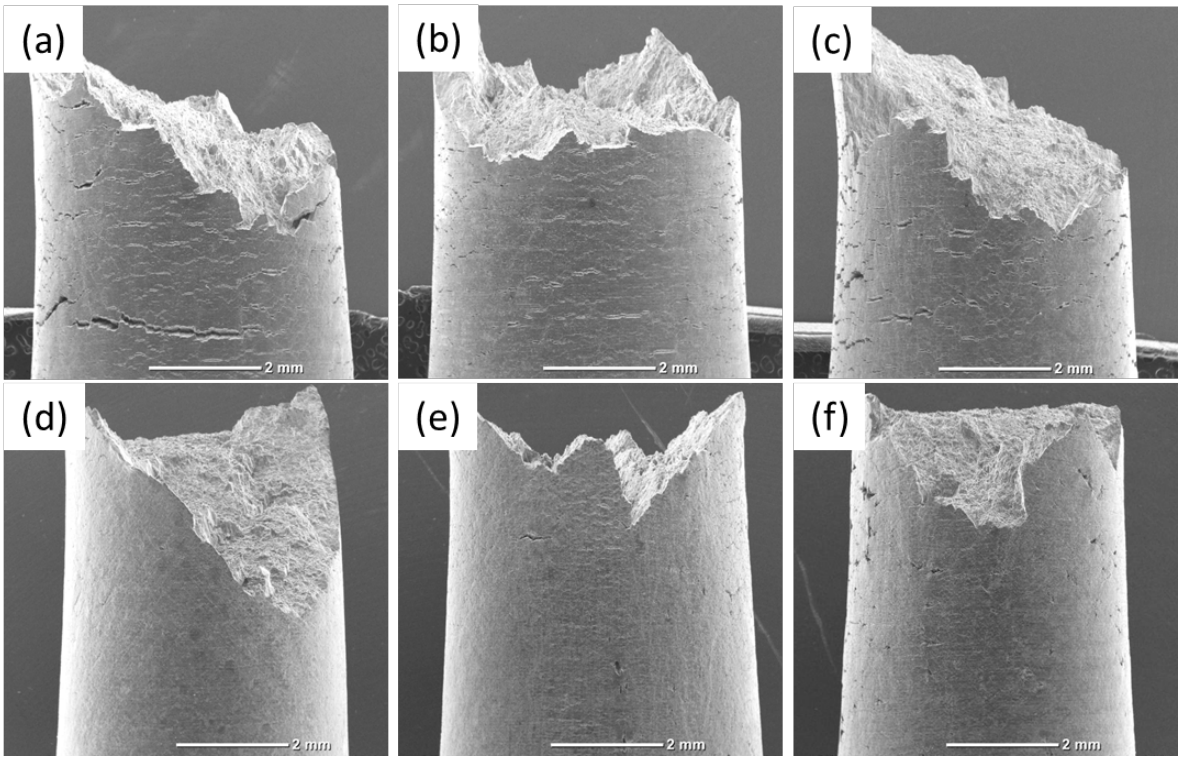

Fig. 7 – The SEM images representing the side surface of the AZ31 alloy specimens SSRT tested in air after pre-exposure to 4% NaCl + 4% $K_2Cr_2O_7$ for 6 – (a, d), 12 – (b, e) and 24 h – (c, f) either as is – (a-c) or after removal of corrosion products – (d-f).

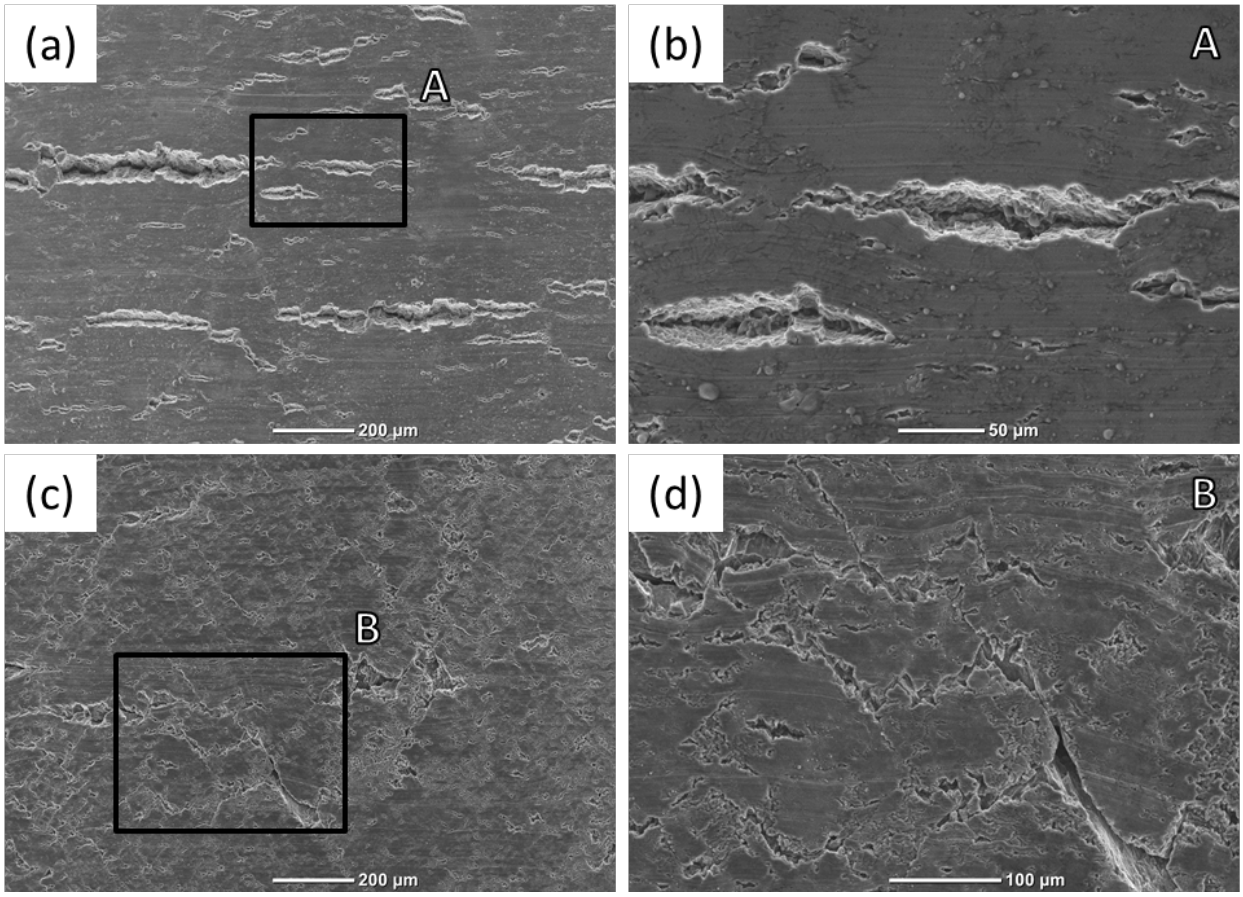

Fig. 8 – The SEM images demonstrating the brittle transverse – (a, b) and ductile shear cracks and corrosion induced flaws – (c, d) on the side surface of the AZ31 alloy specimens SSRT tested in air after 6 h pre-exposure either as are – (a, b) or after removal of corrosion products – (c, d).

3.3.Fractographic analysis

The specimens of the ZK60 alloys tested right after pre-exposure exhibit clearly visible annular brittle zones in the peripheral part of the fracture surface, see Fig. 9a-c. The morphology of such zones is featured by the cleavage-like, Fig. 10a, c, and fluted facets, Fig. 10a, d, e, covered by the cracked film of corrosion products at the edge of the fracture surface, Fig. 10b. The microscopic features of these morphologies in the same alloy have been comprehensively considered elsewhere [24]. The central part of the fracture surface of these specimens is ductile as is witnessed by the characteristic dimpled relief, Fig. 10f. The width of the brittle zone within the fracture surface varies significantly from a few tens up to 700 μm. To account for such a large variation, the size of the brittle component was assessed in terms of the total area and the areal fraction with respect to the entire fracture surface. The quantitative fractographic analysis showed that the total area of the annular brittle zone in the ZK60 specimens increases slightly

with pre-exposure time increasing from 1.5 to 6 h, while the following 12 h of pre-exposure do not affect this property significantly, Fig. 11. On the other hand, the areal fraction of the brittle component grows continuously from 31 to 35 % as pre-exposure time increases from 1.5 up to 12 h.

It should be highlighted that regardless of pre-exposure time, the fracture surfaces of the specimens which were tested after removal of corrosion products are found to be completely ductile, Fig. 9d-f. The careful SEM fractographic examination has revealed no signs of the brittle fracture over the entire fracture surfaces of these specimens. Despite the overall ductile appearance of the fracture surface, the ductility reduction of the specimens with increasing pre-exposure time is manifested by the increase of the fracture surface diameter in Fig. 9d-f. This is in a good agreement with the results of mechanical testing, indicating the decrease of EF of the specimens with removed corrosion products with the increasing time of the pre-exposure.

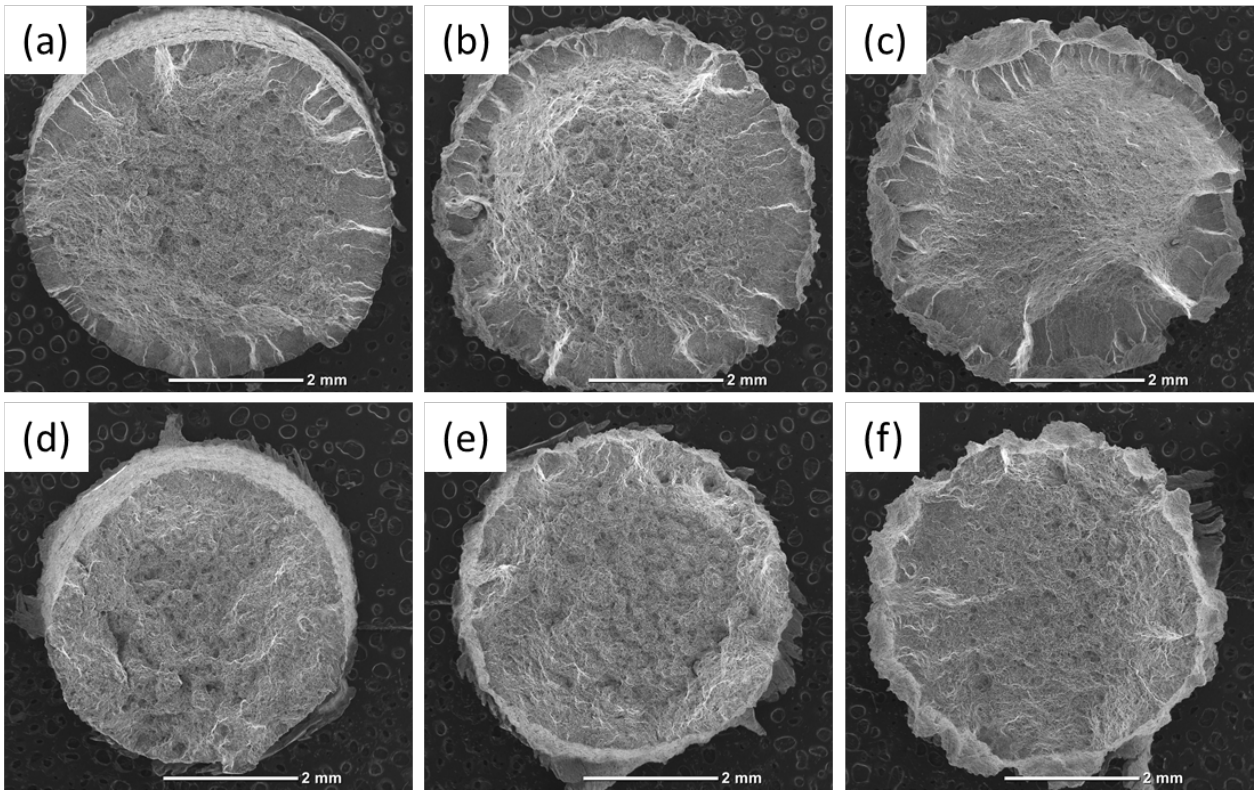

Fig. 9 – The SEM images representing the entire fracture surfaces of the ZK60 alloy specimens SSRT tested in air after 1.5 – (a, d), 6 – (b, e) and 12 h – (c, f) pre-exposure either as are – (a-c) or after removal of corrosion products – (d-f).

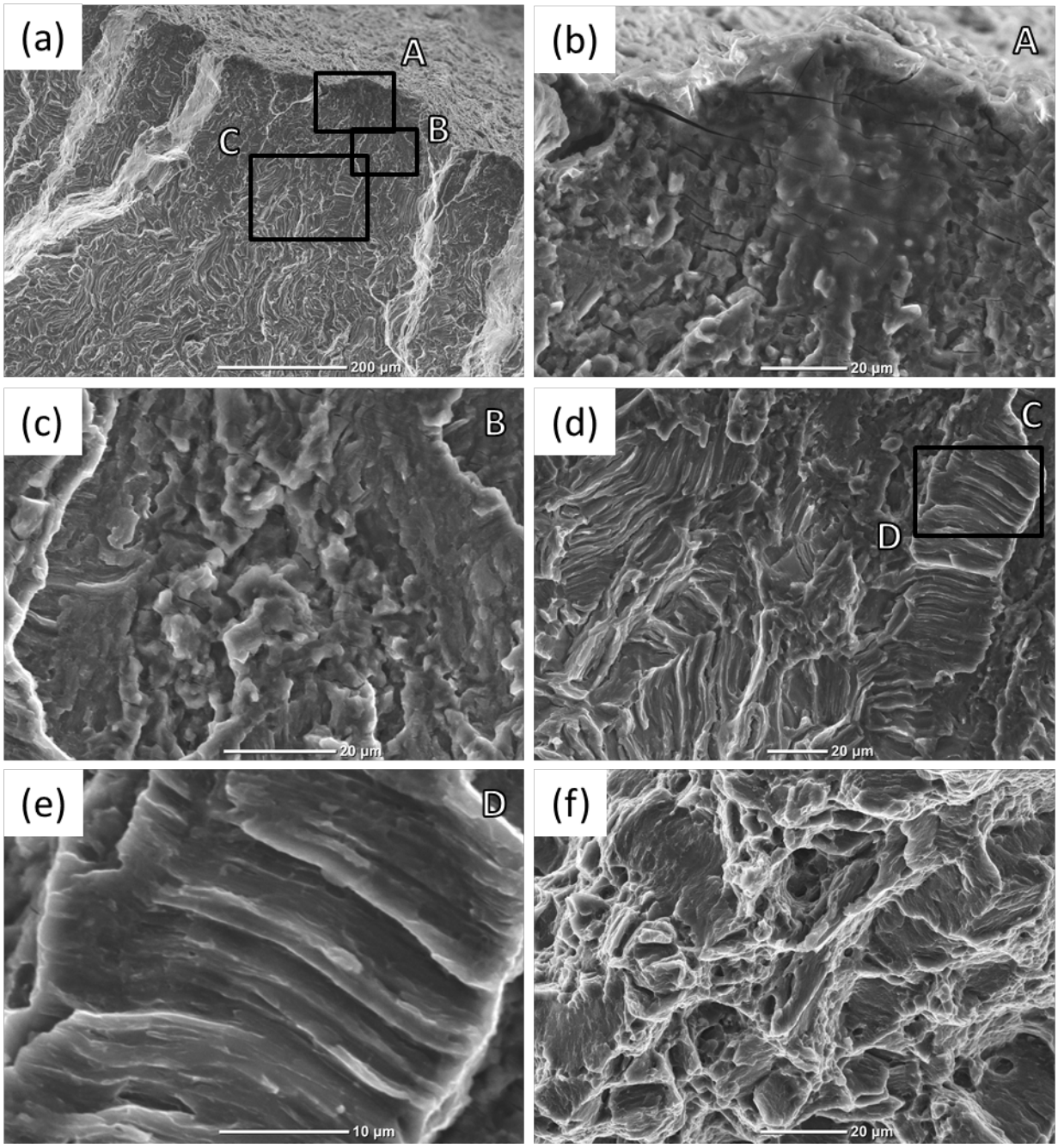

Fig. 10 – The SEM images representing the characteristic fracture surface morphologies of the ZK60 specimen SSRT tested in air after 1.5 pre-exposure to corrosive media: (a) – the close-to-side surface region, (b) – the magnified region marked as “A” in (a) demonstrating the cracked corrosion products film on the fracture surface, (c) – the magnified region marked as “B” in (a) demonstrating cleavage-like morphology, (d) – the magnified region marked as “C” in (a) demonstrating transition region between cleavage-like and fluted morphologies, (e) - the magnified region marked as “D” in (d) demonstrating the minute relief of the fluted facet, (f) – the ductile dimpled morphology of the central part of the fracture surface.

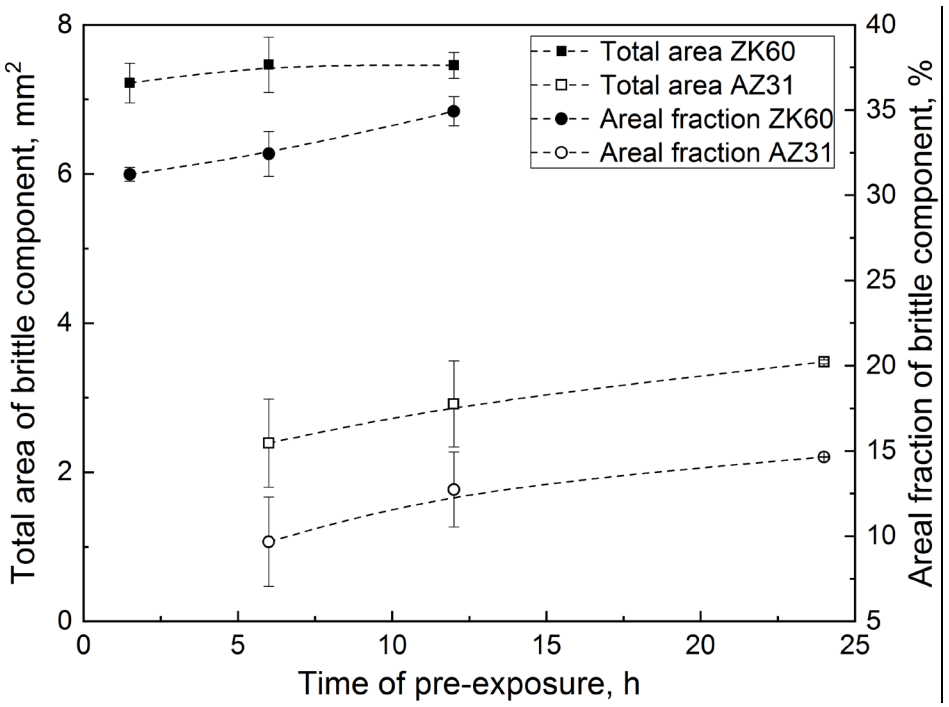

Fig. 11 – The effect of pre-exposure time on the total area and areal fraction of the brittle fracture features with respect to the entire fracture surface for the ZK60 and AZ31 specimens SSRT tested in air after pre-exposure.

The fracture surfaces of the pre-exposed specimens of the AZ31 alloy exhibit the brittle regions along the side surface, and the ductile relief in the central part, Fig. 12a-c and 13. However, in contrast to ZK60, the brittle regions in the alloy AZ31 have a much lesser total area, c.f. Fig. 11, and appear rather fragmented, Fig. 12a-c. So the perfect annular brittle zones such as those on the fracture surface of the ZK60 specimens are not observed in the AZ31 specimens. The increase in pre-exposure time from 6 to 24 h results in a continuous increase of both the total area and areal fraction of the brittle component of the AZ31 specimens, c.f. Fig. 11. Although area-wise, the size of the brittle zone for AZ31 alloy is significantly lower than that for ZK60, the width of this zone in AZ31 varies to a greater extent, and, for some regions, it can occasionally reach of 1.3 mm which is remarkably larger than the maximum width of 700 μm in ZK60. The morphology of the brittle regions of the AZ31 specimens has a completely transgranular appearance featured by the cleavage-like, Fig. 13a-d, and fluted facets, Fig. 13c, e. The intergranular facets, such as those found in AZ31 specimens tested in corrosive media in the previous studies [23,24], are not found in the pre-exposed specimens in the present study. This observation may suggest that the mechanisms of SCC operating in AZ31 during ordinary testing in a corrosive solution and during testing in air after pre-exposure to corrosive media might be different.

The fracture surfaces of the pre-exposed specimens of the AZ31 alloy with removed corrosion products demonstrate the primarily ductile appearance, Fig. 12d-f, though some brittle regions can be occasionally found in the specimens close to the side surface. As can be seen in Fig. 14, all these brittle regions were initiated at the cavities formed on the side surface and elongated towards the interior of the specimen. The characteristic position and the form of such cavities paired with their uneven relief suggest that they are likely the corrosion pits, which were formed during the pre-exposure.

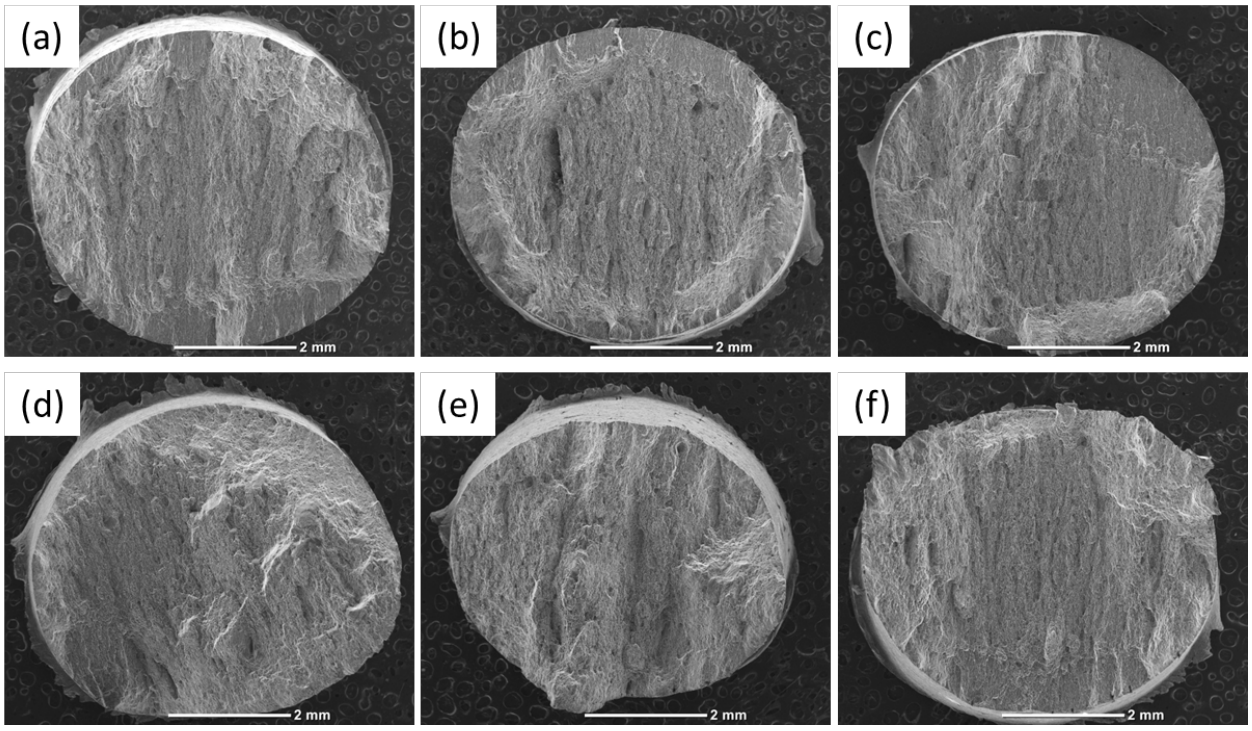

Fig. 12 – The SEM images representing the entire fracture surfaces of the AZ31 alloy specimens SSRT tested in air after 6 – (a, d), 12 – (b, e) and 24 h – (c, f) pre-exposure either as is – (a-c) or after removal of corrosion products – (d-f).

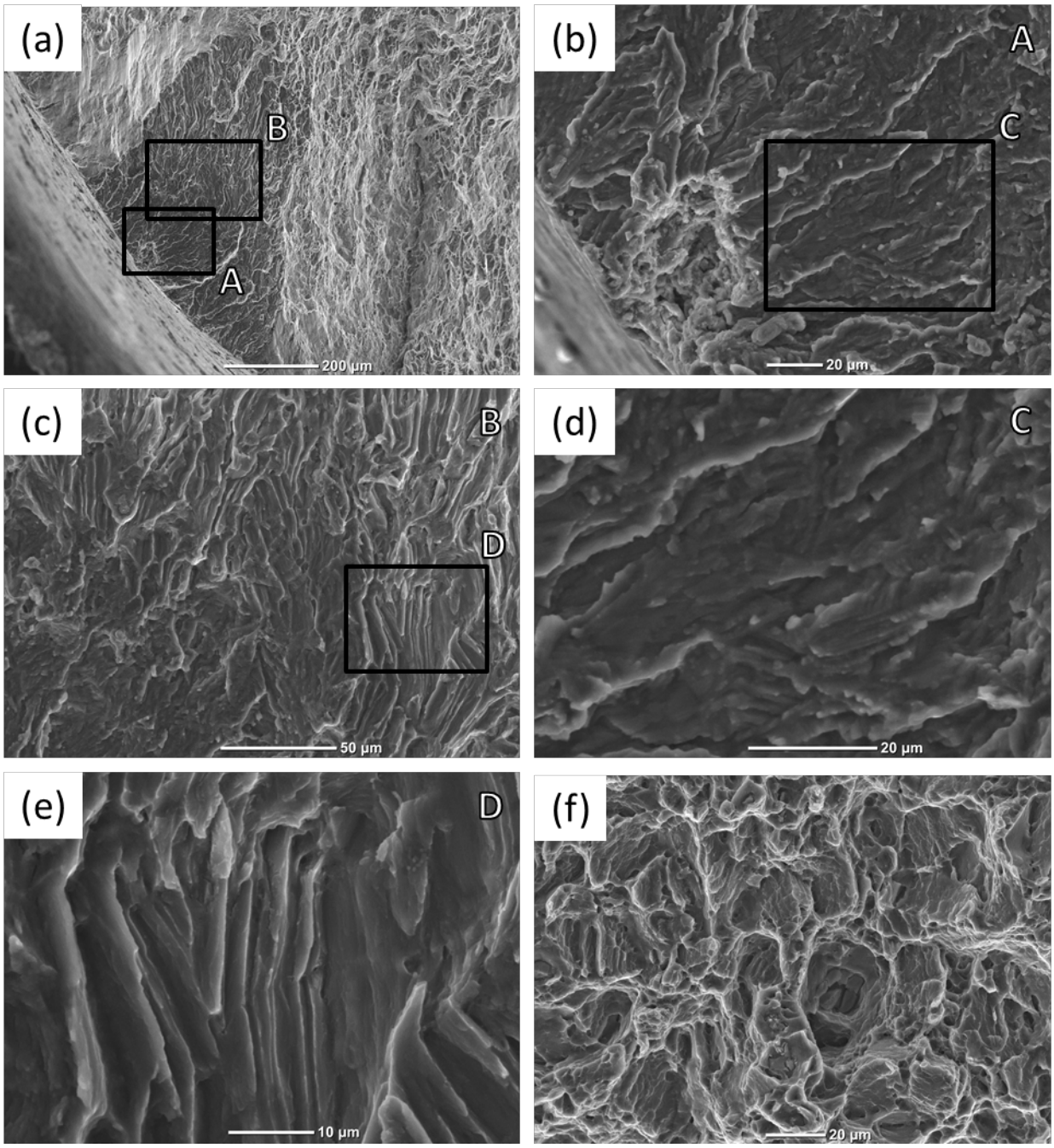

Fig. 13 – The SEM images representing the characteristic fracture surface morphologies of the AZ31 specimen SSRT tested in air after 1.5 pre-exposure to corrosive media: (a) – the close-to-side surface region, (b) – the magnified region marked as "A" in (a) demonstrating the side surface cavity serving as the crack initiation point, (c) – the magnified region marked as "B" in (a) demonstrating transition region between cleavage-like and fluted morphologies, (d) – the magnified region marked as "C" in (b) demonstrating cleavage-like morphology, (e) – the magnified region marked as "D" in (c) demonstrating the minute relief of the fluted facet, (f) – the ductile dimpled morphology of the central part of the fracture surface.

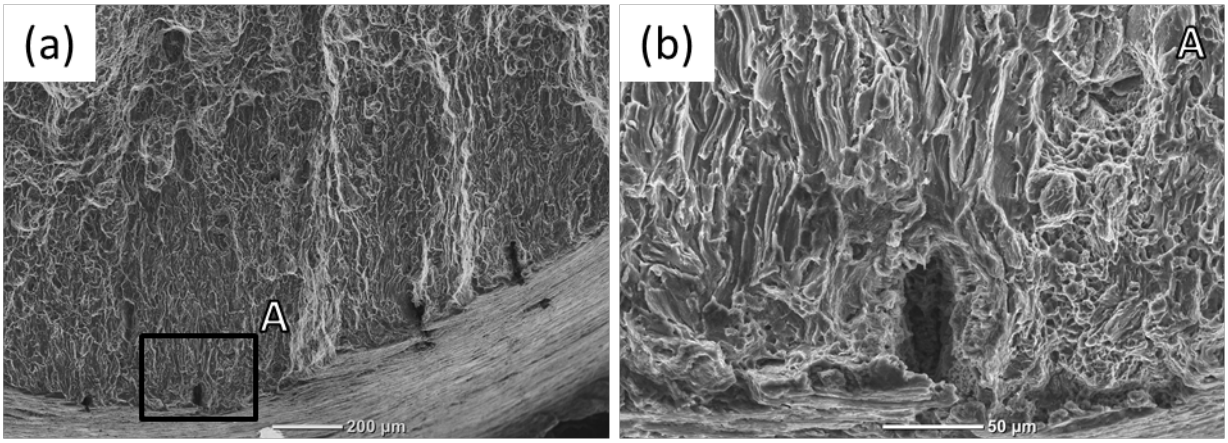

Fig. 14 – The SEM images representing the close-to-side surface brittle regions on the fracture surface of the AZ31 specimen SSRT in air after 6 h pre-exposure and removal of corrosion products.

3.4. Corrosion damage assessment

The considerable corrosion damage of ZK60 specimens, which was evident even from epy superficial side surface observations, c.f. Fig. 3-8, was also quantified by the immersion tests. It can be seen in Fig. 15a that the weight and diameter loss of the ZK60 samples remarkably increases with pre-exposure time. The severity of the corrosion damage can also be assessed by the surface roughness of the samples with the removed corrosion products. These specimens do not contain corrosion products, which can mask the topological features, thus, affecting the apparent roughness of the bare metal. Hence, the undulations of the surface of such samples can be associated with corrosion damage. Indeed, it follows from the Fig. 15b that the roughness of the samples with removed corrosion products is notably higher than that of their counterparts covered by corrosion products. Alike the weight and diameter loss, the surface roughness of the ZK60 samples increases significantly with pre-exposure time due to the progress of corrosion damage. The corrosion damage of the AZ31 alloy is substantially lower than that of ZK60 as is evidenced by the negligible change in weight, diameter and roughness of AZ31 after pre-exposure at any pre-exposure time, c.f. Fig. 15.

In consistence with the results of the side surface observations it is found that the relative weight of corrosion products removed from the ZK60 samples is about one to two orders of magnitude higher than that for the AZ31 samples at the same pre-exposure time, Fig. 16. However, it is worth recalling that the corrosion products were less effectively removed from the AZ31 samples than from ZK60. Hence, the weight of corrosion products for the AZ31 samples is believed to be underestimated. It is found that the increase of pre-exposure time from 1.5 to 6 h

results in the concomitant increase of the relative weight of corrosion products on the ZK60 samples, while further prolongation of pre-exposure time up to 12 h does not affect the weight of corrosion products anymore. The weight of corrosion products deposited on the surface of AZ31 gradually increases with increasing pre-exposure time from 6 to 24 h.

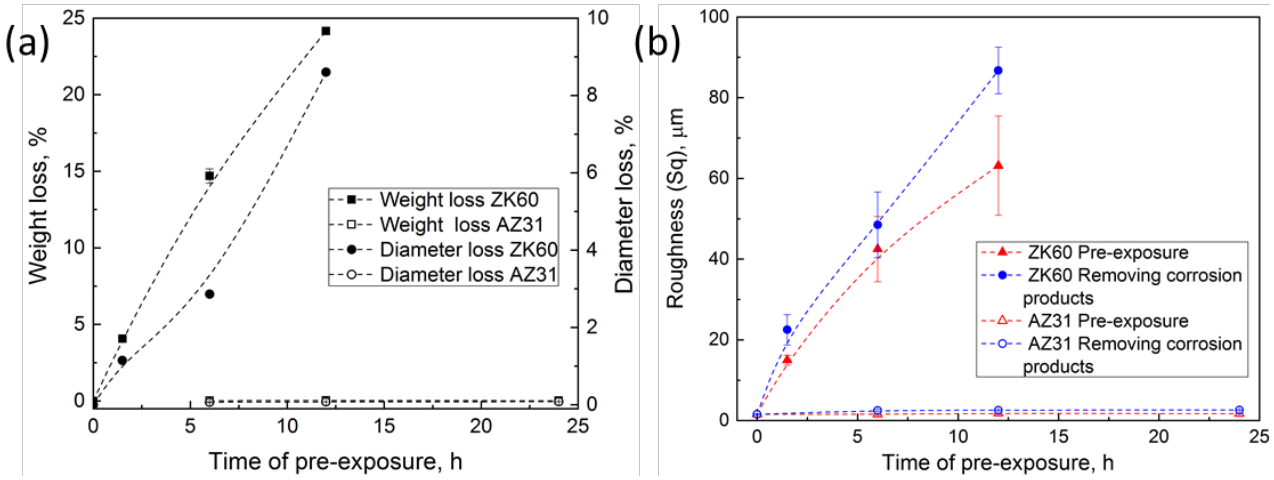

Fig. 15 – The effect of pre-exposure time on the weight and diameter loss – (a) and on the root mean square (Sq) areal roughness of the side surface – (b) of the ZK60 and AZ31 cylindrical samples.

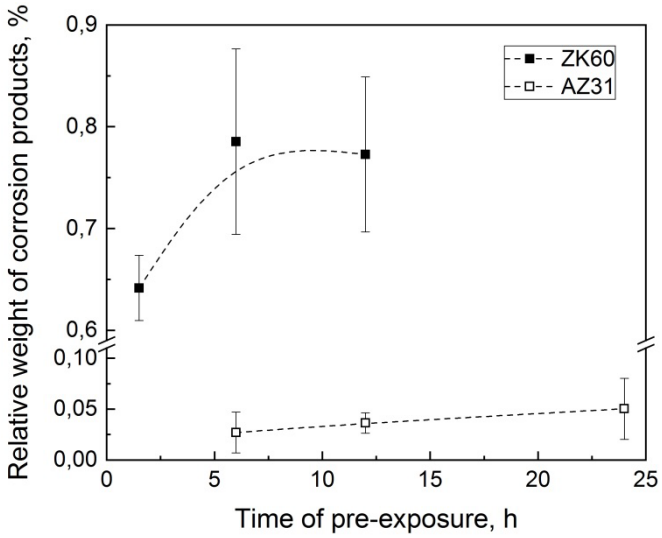

Fig. 16 – The effect of pre-exposure time on the relative weight of corrosion products on the surface of the ZK60 and AZ31 samples.

3.5.Gas-analysis

Extraction curves obtained for the ZK60 and AZ31 samples pre-exposed to corrosive media for different times are provided in Fig. 17. The samples covered with corrosion products

demonstrate extensive desorption of hydrogen in the entire temperature range from 25 to 450 °C. Desorption curves for both alloys contain several pronounced overlapping peaks. The high-temperature peak dominates the hydrogen desorption process at 400-450 °C, whereas the low-temperature peak, which commences systematically at room temperature, fades off well below 300 °C. The features of the extraction curves shown in Fig. 17 are similar to those reported for the same alloys exposed to other NaCl solutions [22–24].

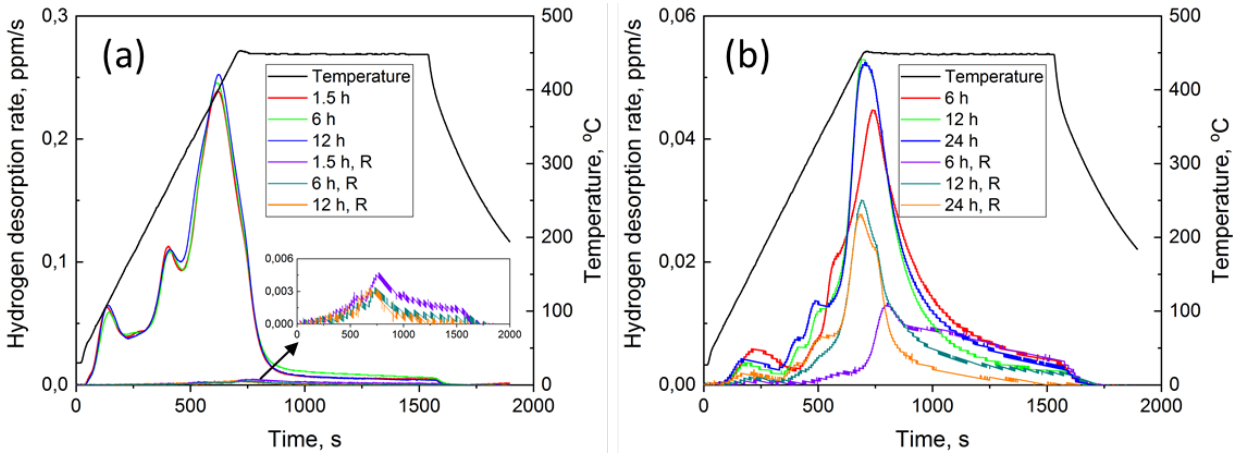

Fig. 17 – The hydrogen desorption curves for the samples of ZK60 – (a) and AZ31 – (b) alloys pre-exposed to corrosive media for different times colour-coded as is specified in the legend. The letter “R” in the legend denotes the samples with removed corrosion products.

Although revealing the exact mechanisms underlying the hydrogen desorption peaks is beyond the scope of the present study, several arguments suggest that these peaks are mainly associated with the corrosion products layer deposited on the sample’s surface. First and most of all, this is strongly supported by the fact that the removal of corrosion products results in the substantial decrease in hydrogen desorption from both alloys over the entire temperature range as is clearly seen in Fig. 17, and as has been convincingly shown in [22–24]. Figure 18 shows that after removal of corrosion products, the total concentration of hydrogen in the ZK60 samples is ranged from 1 to 3 ppm depending on pre-exposure time. This is about one order of magnitude lower than in the counterpart samples covered with corrosion products. The reduction of hydrogen concentration in AZ31 samples due to removal of corrosion products is less dramatic, yet also quite significant. The concentration of hydrogen desorbed from the AZ31 samples with removed corrosion products is about 5 to 6 times higher than in the ZK60 counterparts. One should bear in mind, however, that as was shown above the corrosion products were removed less efficiently from the AZ31 alloy than from ZK60. Thus, the rest of the corrosion products on the AZ31 samples could likely cause a higher concentration of hydrogen. On the other hand,

before the removal of corrosion products, the 5-6 times higher concentration of hydrogen corresponds to the ZK60 samples, which, right after pre-exposure, contain a remarkably higher amount of corrosion products on the surface than the AZ31 samples. Generally, the effect of pre-exposure time on the total concentration of hydrogen in both alloys is found rather weak. The hydrogen concentration of the AZ31 alloy slightly increases with increasing pre-exposure time and correlates with the weight of corrosion products on the surface of these samples. However, for the ZK60 samples, the dependence of the hydrogen concentration on pre-exposure time as well as on the corrosion products weight is less unambiguous.

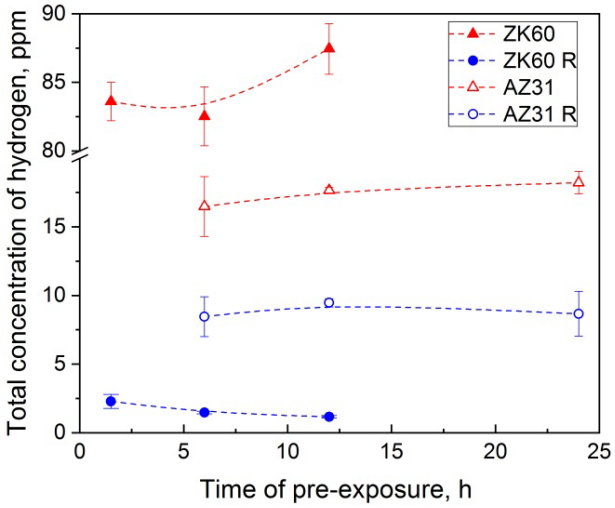

Fig. 18 – The effect of pre-exposure time on total concentration of hydrogen in the samples of ZK60 and AZ31 alloys pre-exposed to corrosive media. The letter "R" in the legend denotes the samples with removed corrosion products.

It should be highlighted that after removal of corrosion products the desorption of hydrogen from both alloys is substantially reduced and is virtually absent in the low-temperature range below 300 °C, as can be seen in Fig. 17. For any pre-exposure time, the concentration of hydrogen extracted from the ZK60 and AZ31 samples below 300 °C did not exceed 0.2 and 0.7 ppm, respectively. It is commonly believed that it is diffusible hydrogen that escapes from metals at the temperatures lower than 300 °C [25]. Thereby, it can be concluded that the concentration of diffusible hydrogen in the samples of both alloys with removed corrosion products is negligible regardless of pre-exposure time. On the other hand, the vanishing of the low-temperature desorption peak after removing corrosion products suggests a high concentration of weakly bonded hydrogen within the corrosion products layer. It is found that about 6 ppm of hydrogen corresponds to this low-temperature peak for the ZK60 samples after 1.5 h pre-exposure. The recalculation of this concentration with respect to the weight of

corrosion products yields that over 1000 ppm of hydrogen located within the corrosion products layer. Interestingly, that this concentration gradually reduces down to about 800 ppm as pre-exposure time increases up to 12 h. The similar estimation of the concentration of hydrogen sitting in the corrosion products for the AZ31 alloy could not be conducted due to the uncertain weight of corrosion products deposited on its samples.

4. Discussion

4.1.Specimens with removed corrosion products

The results of the present study showed that the specimens of the ZK60 alloy pre-exposed to corrosive media for the time longer than 1.5 h suffer from ductility and strength loss which cannot be fully eliminated by the removal of corrosion products. Taken alone, this result can be misinterpreted as supporting evidence for the presence of diffusible hydrogen in the specimens. Indeed, in consistence with the generally accepted explanation for the effect of pre-exposure time on the ductility loss of Mg alloys, one can suggest that the longer pre-exposure allows for deeper penetration of hydrogen into the specimen. This should provide a higher bulk concentration of diffusible hydrogen, causing more significant embrittlement. However, this suggestion can be refuted by two experimental facts established in the present study. The first is that the concentration of diffusible hydrogen in the pre-exposed samples with removed corrosion products is negligible, regardless of pre-exposure time. The second point of controversy is that if one assumes that diffusible hydrogen retaining in the specimens after removal of corrosion products is the main reason of embrittlement, then the retained hydrogen should cause the formation of a brittle fracture surface and side surface cracks in the same way (perhaps, to a lesser extent) as it does in the as-corroded specimens, which were not subjected to the removal of corrosion products. Nevertheless, it was shown above that, in spite of the remaining deterioration of mechanical properties, the pre-exposed ZK60 specimens with removed corrosion products do not demonstrate either the brittle morphology on their completely ductile fracture surface or the brittle transverse side surface cracks. This has been systematically observed independently of the pre-exposure time duration. This observation implies that diffusible hydrogen was either not involved in the degradation of mechanical properties, or, at least, was not the main reason for it in the specimens with removed corrosion products.

The most probable cause of the degraded mechanical response of the ZK60 specimens with removed corrosion products is the corrosion damage, which is found to be increasing with pre-exposure time. As has been shown above, the side surface roughness as well as the cross-section diameter and weight measurements collectively evidenced and reflected the corrosion damage

propagated through the specimen's cross-section. In support of the significance of corrosion damage and its effect on the mechanical response, Figs. 19 a and b show that both the surface roughness and the cross-section diameter nearly linearly correlate with UTS of the ZK60 specimens with removed corrosion products. Thus, the decrease of the apparent UTS value can be simply and most logically explained by the reduction of the cross-section area of the specimens due to corrosion. The EF value also correlates with roughness, Fig. 19a, albeit with the smaller coefficient of regression, while the correlation between EF and diameter reduction is reasonably weak, Fig. 19b. In fact, the relation between EF and roughness does not need to be necessarily linear because the roughness value depends on the depth of corrosion pits which can be harmful by acting as local stress risers [26]. Thus, one can reasonably expect deeper corrosion pits, and, consequently, greater surface roughness and lower EF in the specimens submerged to corrosive media for a longer time.

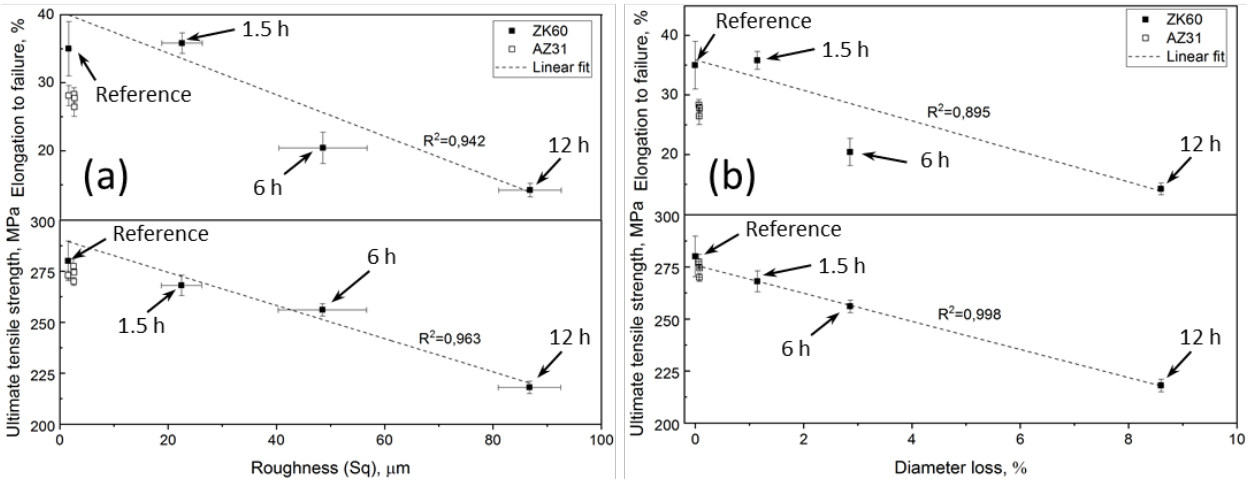

Fig. 19 – The effect of the side surface areal roughness (Sq) – (a) and the loss of cross-section diameter – (b) on the ultimate tensile strength and the elongation to failure of the ZK60 and AZ31 specimens SSRT tested in air after pre-exposure for different durations (see figures indicating pre-exposure time at the arrows) followed by removal of corrosion products. Dashed lines represent the results of the linear regression by the least-square method; the corresponding values of the regression coefficients R^2 are shown.

As it is reasonably expected, the alloy AZ31 demonstrated a notably higher resistance to corrosion and pre-exposure SCC in comparison with ZK60 under the same testing conditions. The roughness and the cross-section diameter of the AZ31 specimens were affected by corrosion to a much lesser extent due to the known overall higher corrosion resistance of the Al-containing AZ31 alloy [27]. In compliance with this observation, the pre-exposed AZ31 specimens exhibit no residual reduction of mechanical properties after the removal of corrosion products. This

statement holds even for those AZ31 specimens, which were immersed into the corrosive solution for a much longer time than ZK60. Thereby, the present findings, as well as the arguments presented in [22], collectively suggest that the reduction of mechanical properties, which is observed in the pre-exposed ZK60 specimens with removed corrosion products, is caused merely by the corrosion damage. Furthermore, the diffusible hydrogen, most likely, does not play an essential role in the fracture mechanism of these specimens. This interpretation provides a rationale to the results of Chakrapani and Pugh [9] and Kappes et al. [17], who also observed the irreversible loss in ductility and strength of the pre-exposed Mg-Al alloys subjected to vacuum annealing and storing in a desiccator.

It should be noted that even after removal of corrosion products, both alloys demonstrated notable evolution of hydrogen at the temperatures above 300 °C for all pre-exposure times. Hydrogen extracting from the samples at such high temperatures is believed to be mainly associated with the decomposition of hydrogen-containing components of corrosion products such as MgH_2 and $Mg(OH)_2$ [7,23,28]. As was stated in the preceding section, a certain amount of corrosion products might retain on the surface even after immersion in the 20% CrO_3 + 1% $AgNO_3$ solution. This is particularly true for the alloy AZ31, for which the procedure of corrosion products removal has been proven less effective than for ZK60 as can be seen in Fig. 4. In consistence with that observation, the AZ31 specimens with removed corrosion products demonstrate 5-6 times higher hydrogen concentration if compared to ZK60, Fig. 18. Besides, in contrast to ZK60, the alloy AZ31 does exhibit side surface cracks, Figs. 7 and 8, and a few brittle regions on the fracture surface, Figs. 12 and 14, although its mechanical properties are not compromised. Apparently, both the enhanced concentration of hydrogen and the appearance of these defects can be attributed to the residual corrosion products on the side surface of the specimens.

4.2.Specimens covered with corrosion products

In conformity with the commonly observed trends [9,16,17], we found that if the corrosion products are not removed prior to SSRT testing, the pre-exposure of Mg alloys to corrosive media results in partial embrittlement accompanied by some loss in ductility and strength, which becomes more and more pronounced with pre-exposure time. Although the irreversible corrosion damage undoubtedly contributes to the degradation of mechanical properties of the ZK60 specimens, it can hardly explain the alternation of the fracture mode from ductile to brittle. This applies particularly to the alloy AZ31, which experiences only insignificant corrosion damage. Thus, besides the corrosion damage, there should be a mechanism responsible for brittle cracking and the concomitant formation of the brittle fracture surface. In cooperation with the irreversible

corrosion damage, this mechanism is supposed to deteriorate the mechanical performance of the alloys. The contribution of both the corrosion damage and brittle cracking to the overall pre-exposure embrittlement is of particular interest.

It is shown in the present study that the area of brittle features on the fracture surface of the ZK60 specimens increases slightly with the immersion time increasing from 1.5 to 6 h, while the further prolongation of pre-exposure does not result in any notable growth of the brittle zone, Fig. 11. This observation implies that the mechanism responsible for brittle cracking in the alloy ZK60 is insignificantly affected by pre-exposure time. Therefore, the decrease in mechanical properties of this alloy with increasing pre-exposure time is likely attributed to the irreversible corrosion damage, rather than to brittle cracking. While the total area of the brittle features on the fracture surface is almost unchanged, the cross-section and the total area of the entire fracture surface of the ZK60 specimens decreases with increasing pre-exposure time due to corrosion. This gives rise to the increasing areal fraction of the brittle fracture, which, in turn, results in the reduction of ductility. Indeed, the perfect inverse linear relationship between EF and the areal fraction of brittle zone is established for both alloys as can be seen in Fig. 20. In contrast to ZK60, the AZ31 alloy demonstrated an appreciable increase in the total area of brittle features with pre-exposure time, while the only insignificant reduction in the cross-section has been documented for this alloy due to corrosion damage. Thus, the increase of the areal fraction of brittle fracture in this alloy should be attributed to the enhanced activity of the brittle cracking mechanism, rather than to the extent of corrosion damage (unlike ZK60). Nevertheless, as follows from Fig. 20, the ductility of both alloys is determined by the areal fraction of the brittle zone regardless of the underlying mechanisms, which are responsible for the formation of the resulting fracture surface.

Despite its relatively minor response to the change in pre-exposure time, the mechanism of brittle cracking apparently results in the strong ductility loss of the ZK60 specimens. This effect is most pronounced within the first hours of pre-exposure, when the corrosion damage has not been developed to the severe stage yet. It is indicated by the steep drop in EF and UTS values of ZK60 specimens after 1.5 h pre-exposure. Similar abrupt reduction of ductility within first hours of pre-exposure has been also documented by other researchers for Mg-Al alloys [9,16]. In the present study, the AZ31 alloy does not exhibit such a dramatic degradation in its mechanical properties as it has been reported in several other studies or as has been found for ZK60. Apparently, this observation is due to the high corrosion resistance of the AZ31 alloy against the 4% NaCl + 4% $K_2Cr_2O_7$ solution, which was not used in other studies on AZ31. On the other hand, the increase of pre-exposure time promotes brittle cracking in this alloy. This is in agreement with the results reported by Kappes et al. [17], who found that the width of the brittle

annular zone in the pre-exposed AZ31B specimens increased from 375 up to 720 μm due to the increase of pre-exposure time from 24 up to 96 h. The width of the brittle zone observed on the fracture surface of AZ31 specimens in the present study is significantly larger than that reported in [17] for the same pre-exposure times. This difference in the results is most likely attributed to the smaller cross-section of the specimens having 4 mm diameter in [17] versus 6 mm in the present study. The differences in microstructure and chemical compositions between the alloys used in [17] and in the present work can also probably account for the variations observed in the fracture surfaces in both studies. To the authors' best knowledge, the ref. [17] represents the only paper where the effect of pre-exposure time on the size of the brittle fracture zone in the pre-exposed Mg-based specimens has been reported so far.

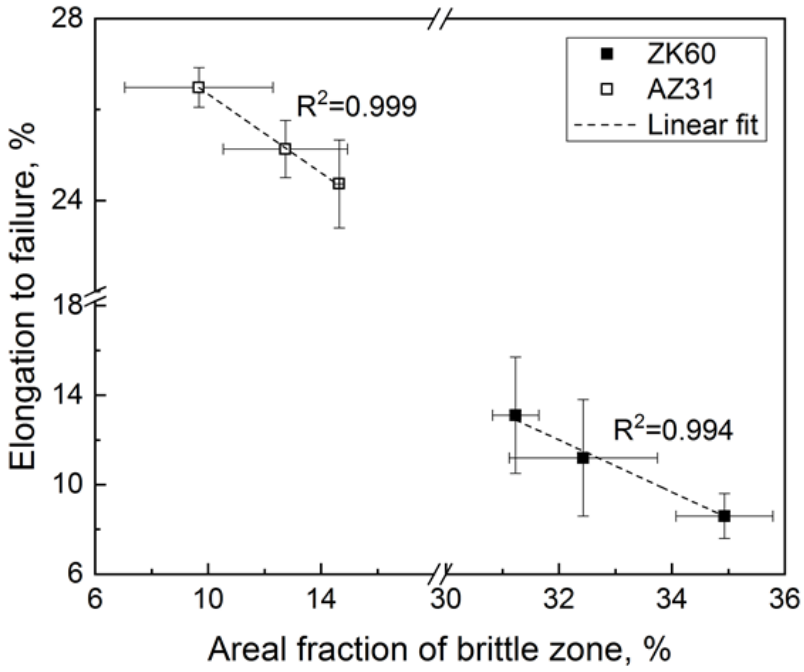

Fig. 20 – The relationship between the elongation to failure and the areal fraction of the brittle zone on the fracture surface of the ZK60 and AZ31 specimens, which were SSRT tested after pre-exposure to corrosive media for different times.

Thereby, both ZK60 and AZ31 alloys experience the reduction in ductility with the increasing pre-exposure time. However, in the ZK60 alloy, this reduction is mainly attributed to the increasing extent of corrosion damage, while in the AZ31 alloy this effect is due to the enhanced activity of the brittle cracking mechanism. It is plausible to believe that the root cause for such a different response of these two alloys to increasing pre-exposure time is related to the corrosion products layer deposited on the surface of the specimens. It was concluded in [22] that the degree of pre-exposure embrittlement of the ZK60 alloy increases with the weight, thickness

and hiding power of the corrosion products film. This conclusion is strongly corroborated by the results of the present study. Specifically, the side surface examination and the gravimetric analysis show that the significantly greater amount of corrosion products, Figs. 3, 4 and 16, and, concurrently, the substantially higher degree of pre-exposure embrittlement are observed in the alloy ZK60 if compared to AZ31. Furthermore, it was shown that both the relative weight of corrosion products and the areal fraction of brittle fracture were just slightly changed in the ZK60 specimens and increased in AZ31, Figs. 11 and 16. Indeed, as can be seen in Fig. 21 the relative weight of corrosion products deposited on the ZK60 and AZ31 specimens pre-exposed to corrosive media for different times correlates linearly with the areal fraction of the brittle features on the fracture surfaces of these specimens. The exact reason for the insignificant growth of the corrosion products layer on the ZK60 specimens with pre-exposure time in unclear as yet. The detailed study of the corrosion behaviour in both alloys in the present corrosive solution is needed to address this issue. However, it was beyond the scope of the present paper.

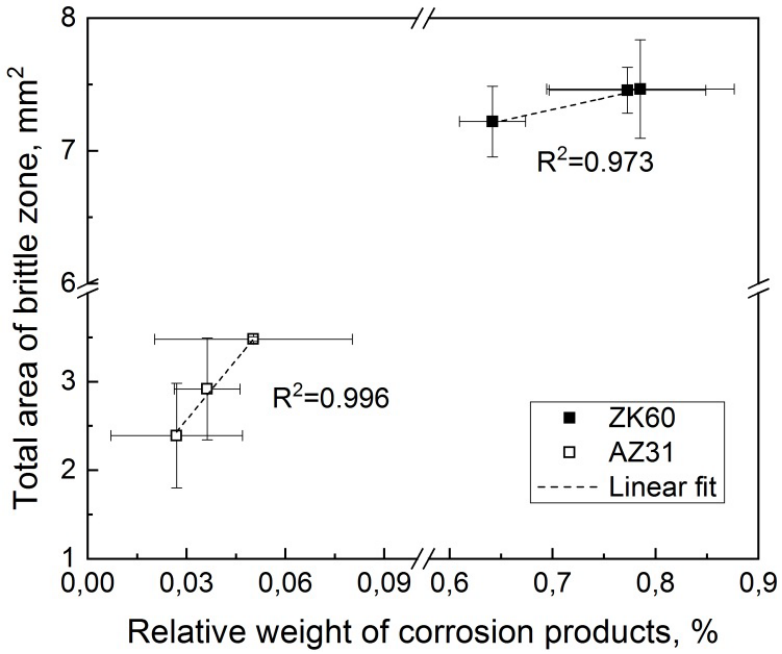

Fig. 21 – The relationship between the relative weight of corrosion products deposited on the specimens of ZK60 and AZ31 alloys after pre-exposure to corrosive media for different times and the total area of the brittle zone on the fracture surface of these specimens.

The rationale standing behind the findings of the present work can be formulated as follows. Because of the high corrosion rate of the ZK60 alloy in 4% NaCl + 4% $K_2Cr_2O_7$, the prominent corrosion damage and the relatively thick corrosion products layer evolve rapidly on the specimens' surface within the first two hours of pre-exposure. The corrosion damage results in the reduction of the specimens' cross-section and the formation of corrosion pits. This, in turn,

leads to the irreversible reduction in strength and ductility, the extent of which increases with pre-exposure time. Concomitantly, the deposition of the thick corrosion products layer activates the brittle cracking mechanism, which forms the brittle zone on the fracture surface and causes the additional significant drop in ductility and the slight decrease in strength. At variance to the effects caused by corrosion damage, all harmful effects produced by the brittle cracking mechanism are reversible and can be eliminated by the removal of corrosion products from the surface of the specimen before mechanical testing. The significance of these effects increases with the increasing amount of corrosion products on the surface. Since, the increase of pre-exposure time from 1.5 to 12 h does not cause the significant growth of corrosion products layer on the ZK60 specimens, the area of the brittle zone on their fracture surface changes slightly, while the progress in the degradation of their mechanical properties is attributed mainly to irreversible corrosion damage, which gets considerably more severe with increasing pre-exposure time. Owing to the much higher corrosion resistance of the AZ31 alloy against the 4% NaCl + 4% $K_2Cr_2O_7$ solution, both the degree of corrosion damage and the amount of corrosion products are much lower in this alloy in comparison to ZK60 at the same pre-exposure time. Thus, after pre-exposure, the AZ31 alloy experiences a notably less severe ductility and strength loss as well as a smaller brittle zone on the fracture surface. However, in contrast to the alloy ZK60, the increase of pre-exposure time does promote the growth of corrosion products layer on the surface of AZ31 specimens but does not cause any significant advance of corrosion damage. Hence, the ductility reduction of the AZ31 alloy due to increasing pre-exposure time is governed primarily by the enhanced activity of the brittle cracking associated with the increased amount of corrosion products, whereas the contribution of corrosion damage to the degradation of mechanical properties is minor.

4.3.The mechanism of brittle cracking

As has been already mentioned, the hydrogen-assisted cracking driven by diffusible hydrogen has long been supposed to be the primary mode of the pre-exposure embrittlement in Mg alloys. The relevance of this mechanism has been challenged in our recent companion paper [22]. It has been concluded, that the role of diffusible hydrogen in brittle cracking promoted by the pre-exposure process is minor. The same conclusion can be drawn from the present results. Firstly, such an inference is directly evidenced by the negligible concentration of weakly-bounded hydrogen in the matrix of the pre-exposed specimens with removed corrosion products. Secondly, it is indirectly indicated by the recovered ductility in these specimens. On the other hand, the healing effect produced by removing corrosion products suggests the crucial role played by the corrosion products layer in the mechanism of pre-exposure embrittlement of Mg

alloys. Thus, it is established that the presence of corrosion products on the specimens' surface is a prerequisite for the activation of the mechanism responsible for brittle cracking in the pre-exposed specimens. This is further supported by the observation that the activity of this mechanism depends strongly on the amount of corrosion products on the specimens' surface. It was suggested in [22], that the corrosion products layer may serve as an accumulator for some "embrittling agent" such as hydrogen or liquid corrosive media which can be probably sealed inside the discontinuities within this layer or in the interfacial volume between this layer and the substrate. Supposedly such embrittling agents can cause the brittle cracking through the AIDE-like mechanism or through the formation of brittle hydrides at the surface of the crack tip. Alternative mechanisms are also possible. For instance, it was shown in section 3.5 that the extremely high concentration of weakly-bounded hydrogen is, indeed, present within the corrosion products layer right after pre-exposure. The exact nature of this hydrogen is unknown, as well as it is unclear whether it is somehow involved in the brittle cracking process. However, it seems plausible to suppose that it is molecular or atomic hydrogen which is accumulated inside the cracks or voids within the corrosion products layer. This hydrogen can assist the initiation and propagation of the cracks. However, no relation is found in the present work between the hydrogen concentration and the loss of ductility or the size of the brittle zone in the fracture surface. It was shown that the concentration of hydrogen in the corrosion products layer of the pre-exposed ZK60 specimens gradually decreases with increasing pre-exposure time. This finding accounts logically for the decrease in the number of side surface cracks in these specimens.

The presence of liquid corrosive media within the corrosion products is less obvious than that of hydrogen, although such a possibility should not be excluded a priori. For example, it was found that the peripheral part of the fracture surface of the pre-exposed specimens was abundantly covered by the crust of corrosion products. Although it is not known whether these corrosion products were formed during pre-exposure or during SSRT testing, one could suppose that the retained corrosive liquid is responsible for the formation of these corrosion products. If the liquid corrosive solution remains within the corrosion products and gives way for corrosion reaction to occur, this reaction can be responsible for the production of gaseous hydrogen, the evolution of which is detected in the form of the low-temperature desorption peak on the extraction curves.

One more effect which can potentially contribute into the brittle cracking in the pre-exposed specimens of Mg alloys is referred to as "corrosion product film-induced stress". This effect is found for many metallic materials including copper [29–31], titanium [32] and iron alloys [33,34]. The point in this mechanism is that the corrosion product film deposited on the

surface can induce a relatively high tensile stress in the substrate, thus creating favorable conditions for the nucleation and propagation of the cracks. To the authors' best knowledge, this effect has not been reported for Mg alloys so far. Nevertheless, taking into account the drastic effect produced by corrosion products on the properties of these materials, it is reasonable to suppose that the corrosion product film-induced stress can be at least partly responsible for the pre-exposure embrittlement of Mg alloys. The increase of such stress with the growth of the corrosion products layer is also well expected. However, as was mentioned in [22] the effect of strain rate on pre-exposure time has to be investigated to distinguish between the contributions from the corrosion product film-induced stress and the mechanisms associated with the potentially embrittling agents. Thus, this will be the scope of our further study.

5. Conclusions

1. The pre-exposure embrittlement of Mg alloys is caused by the cooperative effect of corrosion damage and the brittle cracking mechanism, which is activated by the deposition of the essentially thick corrosion products layer on the specimen surface during pre-exposure.
2. The operation of the brittle cracking mechanism is manifested by the ductility and strength loss as well as by the appearance of the brittle annular zone on the peripheral part of the specimens. Both the degradation of mechanical properties and the size of the brittle zone induced by the brittle cracking mechanism in the ZK60 and AZ31 alloys increases with the increasing amount of corrosion products on the specimen surface. Thus, the increase of pre-exposure time promotes the brittle cracking mechanism, providing that the amount of corrosion products on the specimens' surface increases too.
3. The increase of pre-exposure time promotes corrosion damage as is evidenced by the appearance of corrosion pits, increasing roughness and reducing cross-section diameter and weight of the Mg alloys specimens. The corrosion damage irreversibly affects the ductility and strength but does not alternate the fracture mode of the specimens. The degree of loss in mechanical properties depends on the extent of the corrosion damage, which, for given pre-exposure time, strongly depends on the corrosion resistance of the specific alloy.
4. The pre-exposure embrittlement of Mg alloys can be completely eliminated by the removal of corrosion products from the specimen's surface prior to mechanical testing in air, providing that the irreversible corrosion damage produced during the pre-exposure is insufficient to cause the degradation of mechanical properties.

5. The pre-exposure of Mg alloys to corrosive media does not cause the increase of diffusible hydrogen concentration in the bulk material independently of pre-exposure time; thus, diffusible hydrogen cannot be blamed responsible for the pre-exposure embrittlement phenomenon widely observed in Mg-alloys.

6. The extremely high concentration of weakly-bounded hydrogen exceeding 1000 ppm can be accumulated within the corrosion products layer deposited on the surface of the ZK60 specimens pre-exposed to corrosive media.

7. The AZ31 alloy possesses significantly higher resistance to pre-exposure embrittlement induced by immersion in the 4% NaCl + 4% $K_2Cr_2O_7$ corrosive solution than the alloy ZK60.

Acknowledgements. Financial support from the Russian Science Foundation through the grant-in-aid No. 18-19-00592 is gratefully appreciated.

References

[1] A. Atrens, W. Dietzel, P. Bala Srinivasan, N. Winzer, M. Bobby Kannan, Stress corrosion cracking (SCC) of magnesium alloys, in: Stress Corros. Crack., Elsevier, 2011: pp. 341–380. doi:10.1533/9780857093769.3.341.

[2] A. Atrens, N. Winzer, W. Dietzel, Stress corrosion cracking of magnesium alloys, Adv. Eng. Mater. 13 (2011) 11–18. doi:10.1002/adem.200900287.

[3] N. Winzer, A. Atrens, G. Song, E. Ghali, W. Dietzel, K.U. Kainer, et al., A critical review of the Stress Corrosion Cracking (SCC) of magnesium alloys, Adv. Eng. Mater. 7 (2005) 659–693. doi:10.1002/adem.200500071.

[4] U. Riaz, I. Shabib, W. Haider, The current trends of Mg alloys in biomedical applications—A review, J. Biomed. Mater. Res. - Part B Appl. Biomater. 107 (2019) 1970–1996. doi:10.1002/jbm.b.34290.

[5] A. Vinogradov, V.N. Serebryany, S. V. Dobatkin, Tailoring microstructure and properties of fine grained magnesium alloys by severe plastic deformation, Adv. Eng. Mater. 20 (2018) 1–22. doi:10.1002/adem.201700785.

[6] K.K. Sankaran, R.S. Mishra, Magnesium Alloys, in: Metall. Des. Alloy. with Hierarchical Microstruct., Elsevier, 2017: pp. 345–383. doi:10.1016/B978-0-12-812068-2.00007-2.

[7] M. Kappes, M. Iannuzzi, R.M. Carranza, Hydrogen Embrittlement of Magnesium and Magnesium Alloys: A Review, J. Electrochem. Soc. 160 (2013) C168–C178. doi:10.1149/2.023304jes.

[8] N. Winzer, A. Atrens, W. Dietzel, G. Song, K.U. Kainer, Evaluation of the delayed hydride cracking mechanism for transgranular stress corrosion cracking of magnesium alloys, Mater. Sci. Eng. A. 466 (2007) 18–31. doi:10.1016/j.msea.2007.03.020.

[9] D.G. Chakrapani, E.N. Pugh, Hydrogen embrittlement in a Mg-Al alloy, Metall. Trans. A. 7 (1976) 173–178. doi:10.1007/BF02644454.

[10] N. Winzer, A. Atrens, W. Dietzel, V.S. Raja, G. Song, K.U. Kainer, Characterisation of stress corrosion cracking (SCC) of Mg – Al alloys, Mater. Sci. Eng. A. 48 (2008) 339-351.

[11] N. Winzer, A. Atrens, W. Dietzel, G. Song, K.U. Kainer, Fractography of stress corrosion cracking of Mg-Al alloys, Metall. Mater. Trans. A Phys. Metall. Mater. Sci. 39 A (2008) 1157–1173. doi:10.1007/s11661-008-9475-8.

[12] L.F. Zhou, Z.Y. Liu, W. Wu, X.G. Li, C.W. Du, B. Jiang, Stress corrosion cracking behavior of ZK60 magnesium alloy under different conditions, Int. J. Hydrogen Energy. 42 (2017) 26162–26174. doi:10.1016/j.ijhydene.2017.08.161.

[13] F. Tuchscheerer, L. Krüger, Hydrogen-induced embrittlement of fine-grained twin-roll cast AZ31 in distilled water and NaCl solutions, J. Mater. Sci. 50 (2015) 5104–5113. doi:10.1007/s10853-015-9064-3.

[14] S.P. Lynch, P. Trevena, Stress corrosion cracking and liquid metal embrittlement in pure magnesium, Corrosion. 44 (1988) 113–124.

[15] R.S. Stampella, R.P.M. Procter, V. Ashworth, Environmentally-induced cracking of magnesium, Corros. Sci. 24 (1984) 325–337. doi:10.1016/0010-938X(84)90017-9.

[16] R.G. Song, C. Blawert, W. Dietzel, A. Atrens, A study on stress corrosion cracking and hydrogen embrittlement of AZ31 magnesium alloy, Mater. Sci. Eng. A. 399 (2005) 308–317. doi:10.1016/j.msea.2005.04.003.

[17] M. Kappes, M. Iannuzzi, R.M. Carranza, Pre-Exposure embrittlement and stress corrosion cracking of magnesium alloy AZ31B in chloride solutions, Corrosion. 70 (2014) 667–677. doi:10.5006/1172.

[18] M. Bobby Kannan, W. Dietzel, Pitting-induced hydrogen embrittlement of magnesium-aluminium alloy, Mater. Des. 42 (2012) 321–326. doi:10.1016/j.matdes.2012.06.007.

[19] G.L. Makar, J. Kruger, K. Sieradzki, Stress corrosion cracking of rapidly solidified magnesium-aluminum alloys, Corros. Sci. 34 (1993). doi:10.1016/0010-938X(93)90090-4.

[20] S. Jafari, R.K.S. Raman, C.H.J. Davies, Stress corrosion cracking of an extruded magnesium alloy (ZK21) in a simulated body fluid, Eng. Fract. Mech. 201 (2018) 47–55. doi:10.1016/j.engfracmech.2018.09.002.

[21] S.D. Wang, D.K. Xu, B.J. Wang, L.Y. Sheng, E.H. Han, C. Dong, Effect of solution treatment on stress corrosion cracking behavior of an as-forged Mg-Zn-Y-Zr alloy, Sci. Rep. 6 (2016) 1–12. doi:10.1038/srep29471.

[22] E. Merson, V. Poluyanov, P. Myagkikh, D. Merson, A. Vinogradov, Inhibiting Stress Corrosion Cracking by Removing Corrosion Products from the Mg-Zn-Zr Alloy Pre-Exposed to Corrosion Solutions, Acta Mater. (2020) In press. doi:10.2139/ssrn.3714499.

[23] E. Merson, P. Myagkikh, V. Poluyanov, D. Merson, A. Vinogradov, On the role of hydrogen in stress corrosion cracking of magnesium and its alloys: Gas-analysis study, Mater. Sci. Eng. A. 748 (2019) 337–346. doi:10.1016/j.msea.2019.01.107.

[24] E. Merson, V. Poluyanov, P. Myagkikh, D. Merson, A. Vinogradov, Fractographic features of technically pure magnesium, AZ31 and ZK60 alloys subjected to stress corrosion cracking, Mater. Sci. Eng. A. 772 (2020) 138744. doi:10.1016/j.msea.2019.138744.

[25] A. Laureys, T. Depover, R. Petrov, K. Verbeken, Influence of sample geometry and microstructure on the hydrogen induced cracking characteristics under uniaxial load, Mater. Sci. Eng. A. 690 (2017) 88–95. doi:10.1016/j.msea.2017.02.094.

[26] M. Esmaily, J.E. Svensson, S. Fajardo, N. Birbilis, G.S. Frankel, S. Virtanen, et al., Fundamentals and advances in magnesium alloy corrosion, Prog. Mater. Sci. 89 (2017) 92–193. doi:10.1016/j.pmatsci.2017.04.011.

[27] K. Gusieva, C.H.J. Davies, J.R. Scully, N. Birbilis, Corrosion of magnesium alloys: The role of alloying, Int. Mater. Rev. 60 (2015) 169–194. doi:10.1179/1743280414Y.0000000046.

[28] E.A. Evard, I.E. Gabis, M.A. Murzinova, Kinetics of hydrogen liberation from stoichiometric and nonstoichiometric magnesium hydride, Mater. Sci. 43 (2007) 620–633. doi:10.1007/s11003-008-9002-5.

[29] X.S. Du, Y.J. Su, C. Zhang, J.X. Li, L.J. Qiao, W.Y. Chu, et al., Pre-strain enhances film rupture to promote SCC of brass in Mattsson's solution - A proposal for a film-rupture-induced SCC mechanism, Corros. Sci. 69 (2013) 302–310. doi:10.1016/j.corsci.2012.11.043.

[30] X. Guo, K. Gao, L. Qiao, W. Chu, Stress corrosion cracking relation with dezincification layer-induced stress, Metall. Mater. Trans. A Phys. Metall. Mater. Sci. 32 (2001) 1309–1312. doi:10.1007/s11661-001-0221-8.

[31] W. Wang, Z. Zhang, X. Ren, Y. Guan, Y. Su, Corrosion product film-induced stress facilitates stress corrosion cracking, Sci. Rep. 5 (2015) 1–11. doi:10.1038/srep10579.

[32] X.Z. Guo, K.W. Gao, W.Y. Chu, L.J. Qiao, Correlation between passive film-induced stress and stress corrosion cracking of α-Ti in a methanol solution various potentials, Mater. Sci. Eng. A. 346 (2003) 1–7. doi:10.1016/S0921-5093(02)00529-4.

[33] X.S. Du, Y.J. Su, J.X. Li, L.J. Qiao, W.Y. Chu, Stress corrosion cracking of A537 steel in simulated marine environments, Corros. Sci. 65 (2012) 278–287. doi:10.1016/j.corsci.2012.08.025.

[34] M. Asawa, A. Devasenapathi, M. Fujisawa, Effect of corrosion product layer on SCC susceptibility of copper containing type 304 stainless steel in 1 M H2SO4, Mater. Sci. Eng. A. 366 (2004) 292–298. doi:10.1016/j.msea.2003.08.112.